Worldwide Geometric Satellite Triangulation

HELLMUT H. SCHMID

Geodetic Research and Development Laboratory, NOS, NOAA, Rockville, Maryland 20852

By applying the method of geometric satellite triangulation the three-dimensional positions of 45 stations distributed around the world were determined with an average positional mean error of ±4.5 m. Error theoretical investigations indicate that the result, derived in principle by interpolation into the astronomical right ascension-declination system, is essentially free of significant systematic errors. A comparison of this result of the geometric method with the corresponding result obtained by dynamic satellite geodesy from Doppler data, as computed by the Defense Mapping Agency (DMA) and the Navy, shows excellent overall agreement, with significant discrepancies in a few places on the globe. A combination solution that fully respects the covariance of the photogrammetrically derived directions leads to mass-centered station positions with an average positional mean error of ±3.7 m. The scale of the system, determined by several scalars measured on the earth's surface, suggests an equatorial radius for a best-fitting ellipsoid of 6,378,130 m.

METHOD OF GEOMETRIC SATELLITE TRIANGULATION

The principle of the method of geometric satellite triangulation is based on combining a large number of individual directions to satellites in a three-dimensional triangulation. These satellite directions needed at the stations to be triangulated are obtained by interpolating the individual images of the chopped satellite trail into the framework of the star background present on the photograms [*Schmid*, 1972, 1974].

Directions to the star images are first computed basically as functions of the observing datum, the time of observation (UT1), and the instantaneous pole coordinates. These directions are referenced either to the astronomic right ascension-declination system for a specific epoch or, after appropriate rotation, to an earth-fixed three-dimensional reference coordinate system in which the observation station locations are to be triangulated.

The satellite images are recorded in an arbitrary time sequence, which is, however, common for all stations observing an event. The satellite images are then interpolated into the directions to the stars, i.e., into the background of stars, and thus fixed in the same reference system to which the star images have been reduced. The three-dimensional position of the observing stations is found by assigning to them a location such that the satellite directions emanating from the various stations lead to the determination of the three-dimensional geometry of all observed satellite transits.

It is not necessary, aside from the practical requirements of the field observer, to know in advance the orbit of the satellite. The points of the orbit serve merely as elevated triangulation targets, and only the condition for intersection of corresponding rays is needed to fix the positions of the observation sites. As a consequent requirement, such rays must satisfy the 'geometric condition of simultaneity.' That is to say, they must refer to specific points on the satellite orbit. This condition is automatically met, for example, in case the satellite trail is depicted by the recording of a sequence of flashes emitted by the satellite.

Since to date in practice a sufficient number of such flashes cannot be generated to reduce the influence of scintillation adequately, we photograph the satellite in the portion of its orbit illuminated by the sun. In this method the trace of the orbit is chopped by means of a rotating disk shutter in the camera into a series of time-dependent individual images. For physical as well as technical reasons it is, however, impossible to generate satellite images at the several observing stations that satisfy initially the geometric condition of simultaneity. Basically, it therefore becomes necessary to fit the bundle of directions to the satellite for a particular event as closely as possible to the satellite orbit, which is by its nature continuous. Since only a small portion of the orbit (about 1–2%) is involved, the observed curve may be considered as part of an elliptical orbit obeying the Keplerian laws of motion, a situation that predicates that the satellite directions are referred to an inertial system as approximated, for instance, by the right ascension-declination system.

On the other hand, a solution based on satellite directions referred to an earth-fixed coordinate system requires, because of the earth's rotation, the assumption of a twisted space curve as a model for the satellite orbit.

In such a procedure, satellite triangulation is basically subject to five sources of error. First are the uncertainties associated with the star catalog data. The second that must be considered consists of the accidental errors in time determination for the star and satellite exposures. The third consists of the accidental errors in coordinate measurement of the star and satellite images; fourth, the influence of scintillation acting as an accidental error source; and finally, there is the irregular distortion of the photographic emulsion.

Such a presentation of the error budget assumes first that the corresponding systematic errors are sufficiently small and second that the mathematical model used to reconstruct the photographic process is sufficiently close to reality. Furthermore, the assumption must be valid that the photographed sections of the satellite orbit are in their nature such that in a qualitative sense they may be used as a tool for interpolation. All these assumptions must hold within such accuracy limits that the influence of the remaining imperfections on the triangulation computations remains a magnitude smaller than the propagation of the five cited basic error sources.

Obviously, all further secondary corrections such as pole displacement, astronomic and parallactic refraction, satellite phase angle, and light travel time must correspond to geometric physical reality with such accuracy that the effect of remaining biases is negligibly small.

The rigorous error theoretical treatment of the satellite triangulation method leads, even from this point of view, to a mutually correlated matrix schematic. The individual plates are essentially uncorrelated with respect to the photogram-

metric reduction so far as processing the measured star and satellite coordinates is concerned. However, for all plates introduced into a satellite triangulation system, only one set of reference stars, limited in number and distribution, is available.

Hence the same group of stars appears repeatedly not only on the same plate, as a result of star registration before, during, and after the event, but also such similar groups are recorded on a number of plates.

In the observations for the world net, stars up to eighth magnitude and with maximum mean position errors of 0.4″ were selected from the SAO star catalog. This selection gives us about 20,000 stars at our disposal [*Bossler,* 1966]. With an average frequency of about 100 stars per plate and approximately 3000 plates in the world net, this means that each star appears, on the average, on 15 plates. Since strictly speaking there can only result one pair of corrections for each observed star in the adjustment, the mathematical reconstructions of all the photogrammetric bundles and their orientations are correlated to such a degree that they should really be adjusted as a unit.

In the spatial triangulation of the observing stations the satellite directions are now combined to reconstruct the geometry of the recorded satellite orbit curve. The intersection condition for the rays applied in this process (either direct or indirect by way of fitting to a spatial model of the orbit) contains additional orientation information, similar to the relative orientation in the classical photogrammetric restitution process. But since all photogrammetric bundle parameters that determine directions to the satellite and their orientation quantities are correlated, there results a correlation between all recorded satellite events; i.e., the determination of observing station positions should, together with the determination of all observed satellite orbital curves, be obtained from one common adjustment with the use of the covariance matrix involving all reconstructed photogrammetric bundles and their orientations.

Processing the approximately 2500 plates available in the world net requires the computation of nearly 50,000 interpolation parameters. For the approximately 1100 recorded events, almost 7000 orbital parameters would have to be determined. A simultaneous adjustment of such a large number of correlated unknowns is at present, even with the largest available computer, neither economically feasible nor, because of the required computational accuracy, capable of being realized.

One has therefore to make concessions. From the error theoretical point of view, probably the most serious compromise is the necessity of separately determining the photogrammetric interpolation parameters for each plate, since these parameters determine absolute directions to the interpolated satellite images and are therefore of decisive significance in fixing the spatial positions of the observation stations. In conformance with the weights given with the star data, one pair of corrections for the corresponding star coordinates is obtained in this procedure in each bundle reconstruction adjustment, independent of the number of images of the particular star.

As was mentioned previously, the accidental errors of time designations for the star and satellite recordings must be taken into consideration. In the adjustment for the single camera this requirement is taken care of automatically by carrying corrections to the right ascensions. These being geometrically equivalent to UT1, it is necessary only to compute weights for the introduced right ascension values, the uncertainties in time associated with the recorded instants of observation being taken into account. For the instrumentation used in the world net this accidental timing error amounts to less than a millisecond so far as the registration of the shutter action is concerned. Since the available UT1 is in itself scarcely better than ±2 ms (which acts as a system error in the orientation for the individual plate), the assumption of a ±3-ms overall uncertainty in the determination of time for the star exposures seems reasonable. The inaccuracy of a direction corresponding to this time uncertainty is ±0.045″, a magnitude considerably less than the photogrammetric measuring accuracy obtained with the BC-4 system and the 450-mm lens, hence negligible.

A similar conclusion can be drawn with respect to the influence of random errors of the synchronization procedure on the satellite images. By means of periodic control of timing the instants of observation at the various stations are fixed in relation to each other within at least ± 100 μs. The most critical situation would arise for the Echo satellite with a speed of 8 km/s and minimum distance of 1000 km, where 100 μs corresponds to a change in direction of ±0.16″. With the Pageos satellite used in the world net, because of its greater distance and consequent slower speed, a timing error of ±100 μs results in a maximal direction uncertainty of only ±0.04″. Although this is negligibly small, a calculation employed in the adjustment discussed later on, which is designed primarily to eliminate scintillation with polynomial curve fitting, serves to adjust as well any existing random timing errors in the synchronization.

Existing correlations between the separately reconstructed bundles of directions to stars are, as was detailed above, neglected. Thus for each single-camera computation, individual parameters are determined for the interpolation model including, of course, the covariance matrix associated with these parameters, which is of basic significance for further evaluations.

In the step of the adjustment that now follows, the locations of the observing stations are computed. Their position in space is fixed by the condition that the bundles of directions to the satellite issuing from these stations must lead to the geometry of all satellite orbital curves that have been recorded. Since each bundle of directions is obtained basically by the interpolation of the corresponding satellite images into the relevant interpolation model and since these models are now no longer correlated, it follows that the individual satellite orbit determinations are likewise uncorrelated. This situation results in an essential simplification of the data processing, since the orbit determinations can be processed sequentially and care need only be taken that their cumulative effect bears on the station determination.

The condition of intersection on which, as was mentioned previously, is based the determination of the geometry of the observed satellite orbits (either directly or indirectly by way of a fit to a spatial orbital model) basically contains additional information for determining the parameters of the relevant interpolation models. It follows that not only the coordinates of the stations and the parameters specifying the geometry of the satellite orbit must appear as unknowns in the adjustment, but so must all parameters of all interpolation models involved, together with their individual variance-covariance matrices referred to above.

The resulting system of normal equations is $Bv = \Delta$ with a range in weights P from zero to infinity. By designating the

v_l	v_o	v_{x_s}	v_x	k_l		
$-P_l$				I		0
	0			B_o^T		0
		0		$B_{x_s}^T$	=	0
			0	B_x^T		0
I	B_o	B_{x_s}	B_x	0		Δ_l

Fig. 1. Basic normal equation system corresponding to observation equations $Bv = \Delta$. The weights P range from 0 to ∞. Additional conditions are as follows: **O** is the solution vector of single-camera adjustment, with P_o, and **X** may be given from independent surveys, with P_x.

vector of corrections to the measured satellite image coordinates by v_l, the correction vector for the previously computed bundle interpolation parameters **O** by v_o, the correction vector for the approximated satellite orbital positions by v_{x_s}, and finally the correction vector for the approximated station coordinates by v_x, the corresponding normal equation system can be written as is indicated in Figure 1. With **X**, supplementary conditions are introduced that may exist between the stations to be triangulated such as, for example, measured distances for scale determination. A description of the notation and the mathematical theory outlined here will be found in the work by *Schmid and Schmid* [1965]. The specific application above is detailed in the work by *Schmid* [1972, 1974].

Figure 2 shows the normal equation system after these functional relations have been introduced. The corresponding set of correlates is designated by k. The system reduced down to satellite orbit and station coordinates is given in the lower portion of Figure 2.

Because the image coordinates can be expressed as functions of the interpolation parameters describing the photogrammetric bundle, of the coordinates of the satellite position, and of the relevant coordinates of the observing station, it is possible, since the individual bundle reconstructions are uncorrelated, to replace the correction vector to the interpolation parameters by a corresponding correction vector to the image coordinates, this process thus reducing decisively the number of unknowns to be carried.

As is apparent from the lower portion of Figure 2, this computational procedure is completely rigorous only when the expression Δ_0 is carried along on the right-hand side of the reduced normal equation system, i.e., with the vector of absolute terms; hence a rigorous elimination of the O parameters is not possible. However, since in the first iteration loop the O values as obtained from the single-camera adjustment are introduced into the triangulation adjustment as approximation values, Δ_0 is initially a zero vector. This means that the elimination of the O parameters is valid to within the first order of the Δ_0 terms. Moreover, owing to the large number of absolute control points (in our case about 100 stars per plate) the influence of the orientation contribution resulting from the intersection condition is quite small, so that the considerable gain in simplicity derived by the elimination of these parameters in the triangulation adjustment justifies the procedure.

This simplification leaves the unknowns that are to be determined by means of the condition of intersection of the rays: the coordinates of the observing station for one and the parameters describing the geometry of the satellite orbital curves. From a conceptual point of view it follows that the bundles of directions to a satellite assigned to a particular satellite pass must fit themselves as closely as possible in the sense of an adjustment to the orbital curve, which is subject first of all to the geometric consequences of Kepler's first law, according to which the orbit can be expressed in an inertial system by the equation of an ellipse.

Furthermore, the fitting process must do justice to the dynamic content of Kepler's second law, according to which the true anomaly is a function of time. It seems convenient in

Introducing $\Delta_o = \vec{O} - O^\circ$ *and* $\Delta_x = \vec{X} - X^\circ$

v_l	v_o	v_{x_s}	v_x	k_l	k_o	k_x		
$-P_l$				I				0
	0			B_o^T	I			0
		0		$B_{x_s}^T$				0
			0	B_x^T		I	=	0
I	B_o	B_{x_s}	B_x	0				Δ_l
	I				σ_o			Δ_o
			I			σ_x		Δ_x

$\sigma_o = P_o^{-1}$

$\sigma_x = P_x^{-1}$

After elimination of v_l v_o k_l k_o *and* k_x

v_{x_s}	v_x	
$-B_{x_s}^T(\sigma_l + B_o\sigma_o B_o^T)^{-1}B_{x_s}$	$-B_{x_s}^T(\sigma_l + B_o\sigma_o B_o^T)^{-1}B_x$	$B_{x_s}^T(\sigma_l + B_o\sigma_o B_o^T)^{-1}(\Delta_l - B_o\Delta_o)$
$-B_x^T(\sigma_l + B_o\sigma_o B_o^T)^{-1}B_{x_s}$	$-P_x - B_x^T(\sigma_l + B_o\sigma_o B_o^T)^{-1}B_x$	$P_x\Delta_x + B_x^T(\sigma_l + B_o\sigma_o B_o^T)^{-1}(\Delta_l - B_o\Delta_o)$

Fig. 2. The normal equation system augmented with additional constraints. The lower portion shows the reduced matrix after elimination of the auxiliary parameters v_l, v_o, k_l, k_o, and k_x.

the application to develop the true anomaly as a series in the eccentricity and the mean anomaly. Basically speaking, one can say that the first Keplerian law accomplishes the fit of the bundle perpendicular to the direction of the orbital curve and the second law along the orbit curve. Kepler's third law cannot be made use of because in the first place the orbital period of the observed satellite is not known. Moreover, the balloon satellite with its typically unfavorable mass-surface ratio is exposed to disturbing influences such as residual atmospheric pressure and the sun's radiation pressure, so that the orbital period could yield only limited information in a geometric sense. All computational schemes must furthermore take into account the fact that the recorded times for satellite imagery refer to the instants of exposure and these data must therefore be corrected for light travel time and geometrically for earth rotation during this light travel time before they can be processed further with the application of the principles of celestial mechanics.

The practical application of orbital determination by means of bundle fitting is faced with two further obstacles. In order to obtain the required accuracy in the final result a large number of satellite images is needed in the adjustment to reduce sufficiently the scintillation effect. In the world net the number of images averages 300 per plate. Since the corresponding 300 directions are derived from one and the same group of interpolation parameters, they are correlated, which means that for each of the satellite direction bundles to be introduced into the fit a 600 × 600 completely filled covariance matrix must be taken into consideration. If the event has been observed by more than two stations, this leads very quickly to undesirably large demands on the memory capacity of the computer. Even more decisive is the fact that the scintillation effect depends on the meteorological conditions during the event, which can be quite different at the contributing stations. To prevent this 'noise' from being averaged between the contributing stations to an event in the triangulation adjustment, the appropriate weight matrices for the individual direction bundles must be computed by using the mean scintillation characteristic for each station. This quantity is, however, in the evaluation method under discussion not yet available.

As an alternative to the bundle-fitting concept one could also fix the satellite orbital curve by smoothing the spatial coordinates of the triangulated satellite points with polynomials as functions of time [*Wolf*, 1967]. Such a solution assumes that the orbital curve is designated by a series of short-duration flashes emitted from the satellite, the time sequence of the flashes being sufficiently well known. Only then will there be recorded images on the individual plates that lead to the triangulation of the corresponding orbital points. On the other hand, if, as is necessary for practical reasons at this time, the satellite images are produced on the various plates by chopping the trail of the continuously illuminated satellite with a rotating disk shutter into separate points, then one would first have to compute the necessary light travel times iteratively with approximated satellite positions. In principle this procedure would give sufficient information to interpolate on each photogram the event image points satisfying the geometric condition of simultaneity. From an error theoretical standpoint, however, such interpolation is open to question for the very reason that the position of the individual images is influenced to different and unknown extent by scintillation. From the computational standpoint, still another disadvantage accrues to this solution in that all the satellite directions on the selected plates are correlated, this situation leading to variance-covariance matrices the consideration of which would require an intolerable amount of memory space. The theoretical and practical difficulties of the above method of solution are circumvented by modifying the approach and evaluating each plate independently to the greatest extent possible.

This concept is valid also from the standpoint of error theory and is based on the fact that the measurements at a given observing station, i.e., the photogrammetric registration of the star images and satellite orbit together with the relevant recordings of time, are self-sufficient in the sense that the information so obtained is completely independent of and not influenced by the fact that similar operations have been carried out at other stations. Transforming these measuring data into time-correlated satellite directions requires only the additional assumption that the satellite orbital curve is by nature continuous.

With knowledge of the geometric-dynamic properties of the photographed portion of the satellite orbit as described above, it should be possible to postulate the form of this trail on the photogram in direction of the trail and at right angles to it in terms of the central perspective laws, light propagation time, and the aberration due to the earth's rotation. The formalization would lead to an infinite series expansion in which higher-order terms could be neglected. An adjustment to this theoretical model of the orbital projection could then be made by fitting the satellite images to it. Another possibility, and the one adopted here, is to smooth the satellite images with polynomials. Just as the triangulated spatial coordinates of discrete orbital points can be fitted to polynomial functions of time, the recorded sequence of time-related satellite images can similarly be smoothed, the result being the positions of the satellite on the photogram as a function of time. A curve fit is justifiable all the more from the standpoint of error theory inasmuch as the simplest conceivable projection model exists between the orbit, continuous by nature, and the corresponding satellite image sequence. The measured satellite image coordinates, by means of the bundle reconstruction parameters, as obtained from an adjustment based on reference stars and their images, are therefore first of all reduced to the concept of a rigorous central perspective, i.e., the concept of an ideal photograph. Then one applies the principle of least squares to compute best-fitting polynomials. To the extent that the central perspective nature of the images of the satellite orbital points has been reproduced, this adjustment has the function of neutralizing the random errors of the comparator measurements, random emulsion shrinkage, and scintillation effects. In addition, it yields in the form of statistical functions an indication of the accuracy of the smoothing polynomials.

In order to verify the required degree for these polynomials, 380 satellite space coordinates for a simulated Pageos orbit at intervals of 0.8 s were recorded, which corresponds to the average length of the Pageos arc observed with the BC-4 camera. The satellite orbit was integrated with a tenth-order Cowell-Störmer process. The earth's gravity field was introduced by means of an expansion in spherical functions to the fourth degree and fourth order by using the coefficients of the Smithsonian Institution standard earth [*Lundquist and Veis*, 1966]. Radiation pressure of the sun and attraction of the moon and sun were also included in the integration computations. The resulting coordinates of satellite positions were then transformed into a geostationary system.

Six fictitious observing stations (Figure 3) were distributed

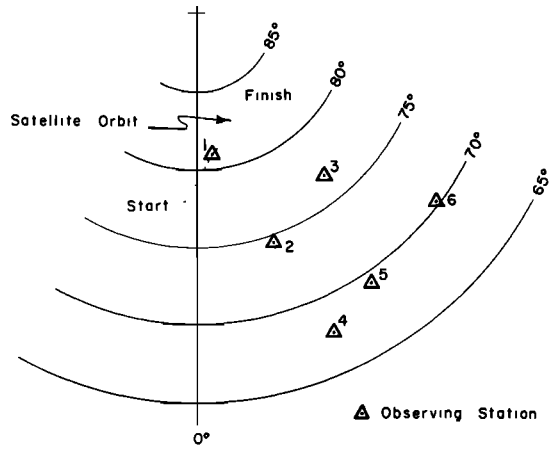

Fig. 3. Schematic representation of the portion of the satellite orbit observed and the typical location of observing stations.

in relation to the computed orbit to simulate essentially the geometric distribution of stations in practice. By applying the time of light propagation for each of the 380 fictitious points of the orbit, corresponding plate coordinates were computed at each of the six stations to reproduce an exact central perspective mapping of the orbital geometry. These plate coordinates were then subjected to polynomial curve fits from the first to the eleventh degree in sequence. The resulting mean errors of the computed coordinates after adjustment are listed in Table 1, σ_x referring to the coordinate component in direction of the trail and σ_y to the component at right angles to the trail.

From Table 1 it is seen that the required accuracy can be obtained with a polynomial of the fifth degree along the trail and of the fourth degree across the trail. At the same time, no undesirable effect of 'oversmoothing' is apparent with polynomials of higher degree, at least up to the eleventh. This degree is of consequence in that from an adjustment polynomial of the nth degree, only $n + 1$ computed values can be used; otherwise, the corresponding covariance matrix becomes singular, whereas the use of fewer values does not exhaust the available information content completely.

In processing the world net, polynomials of the sixth degree are used in smoothing both x and y, so that seven fictitious directions can be used in the final triangulation provided that the trace of the portion of the satellite orbit common with other stations extends over the whole plate. Thus the polynomials provide the adjusted location of the satellite trace as a function of the recorded time. This relation is very useful, since it simplifies the application of the influence of time corrections such as clock differences and light propagation. It is merely necessary, after having transformed a selected satellite orbital time to a corresponding time of registration on the plate, to compute from the relevant polynomial x and y coordinates for the corresponding fictitious plate image with this latter time. By using this procedure on all photograms that have observed a common event a fictitious image is obtained on each photogram satisfying the geometric condition of simultaneity. An approximate preliminary triangulation of the relevant orbital points will be needed to determine for each registered orbital image the variable propagation time of light. It should be noted in this connection that an error of 3 km in the approximated distance will create an error of only 10 μs in the time. Along with the coefficients of the curve fit polynomials one obtains the mean dispersion of the individual images and hence the variance-covariance of the polynomial parameters. Since the fictitious satellite image positions corresponding to specified times are computed as functions of the polynomial parameters, the corresponding error propagation computation will produce their variance-covariance matrix, which displays rigorously the correlations among the individual satellite images resulting from the polynomial smoothing. If seven such fictitious satellite images are used, as, for example, in the world net, a 14 × 14 covariance matrix for these points must also be computed.

At this stage the following evaluation data are available for each satellite orbit observation at a station: (1) the 20 bundle parameters describing the interpolation model, including the exterior elements of orientation, and the associated covariance matrix (in this case, of dimensions 20 × 20) scaled to an a priori introduced error of unit weight; and (2) the pairs of coordinates for the selected fictitious satellite images (in the present case, seven pairs) together with their 14 × 14 covariance matrix, also referred to the error of unit weight mentioned in (1).

The last processing step, computing the three-dimensional geometry of the observing stations, amounts basically to determining the spatial directions corresponding to the fictitious satellite images in order to triangulate the satellite orbit points and all the observation sites by means of an adjustment, subject to the condition that the sum of squares of weighted corrections to the fictitious satellite image coordinates be a minimum. The weight matrices of the satellite direction bundles are compounded at each station by the joint influence of the covariances of the relevant interpolation parameters

TABLE 1. Curve Fit of 380 Fictitious Satellite Images With Polynomials of Degree 1-11

Observation Station	Degree of Polynomial	σ_x, μm	σ_y, μm
1	1	404,166	215,720
	2	53,445	1,853
	3	1,267	289
	4	90	6
	5	3	1
	6	0	0
2	1	461,861	133,736
	2	54,919	964
	3	1,479	166
	4	99	4
	5	4	0
	6	0	0
3	1	226,233	169,385
	2	50,510	229
	3	709	204
	4	76	2
	5	2	0
	6	0	0
4	1	494,437	57,121
	2	53,362	209
	3	1,571	39
	4	99	0
	5	4	0
	6	0	0
5	1	356,618	82,163
	2	51,751	223
	3	1,116	77
	4	85	1
	5	3	0
	6	0	0
6	1	145,585	157,387
	2	48,951	476
	3	458	184
	4	70	0
	5	1	0
	6	0	0

Parameter x is in direction of the trail; y is normal to it. For polynomials of seventh to eleventh degree, all ϵ - tries are zero, as they are for the sixth degree.

(point 1 above) and the covariances of the plate coordinates of the fictitious satellite images (cf. point 2 above).

Whenever additional a priori given information relative to the geometry of the observing sites, such as spatial distance between them (as for scale determination), position coupling between adjacent stations (eccentric reductions), or the like, is used as input data, such data can be introduced into the adjustment without difficulty after the computation of the necessary functional weights, referred of course to the a priori selected error of unit weight. This is true also for the case where additional geometric data will become available through, for example, laser distance measurement between satellite and station.

In the world net, such scalars will be introduced in the form of measured distances of edges of the world net polyhedron in primarily the United States, Europe, Africa, and Australia, as shown in Figure 4.

These basic ideas underlying the error budget of geometric satellite triangulation are presented here in explanation of the error theoretical considerations that lead to the applied adjustment algorithm. Moreover, by pointing out computational possibilities differing from the present solution and leading eventually to completely rigorous adjustment and error propagation, it is hoped that impetus will be given to perfecting the developing method of geometric satellite triangulation.

In the next section some results on the accuracies in the various evaluation phases obtained in the processing of the observational data for the world net will be reported.

Error Theoretical Considerations and Analysis of the Results

Analysis of the Essential Sources of Error and the Error Propagation Into the Spatial Triangulation

In the preceding section it was shown that in essence the method of geometric satellite triangulation is subject to five random error sources. The accidental errors from these sources arise in connection with (1) the comparator measurements of star and satellite images, (2) the reference data from the star catalogs, (3) the designated times of the star and satellite recordings, (4) atmospheric scintillation affecting the directions to the recorded star and satellite orbit points, and (5) accidental emulsion shifts generated in the process of developing the plate.

This idealized situation will, however, only exist to the degree to which during the field observations and in the data processing, sufficient precautions are exercised either to model the following systematical error sources or to eliminate them by corresponding operational procedures.

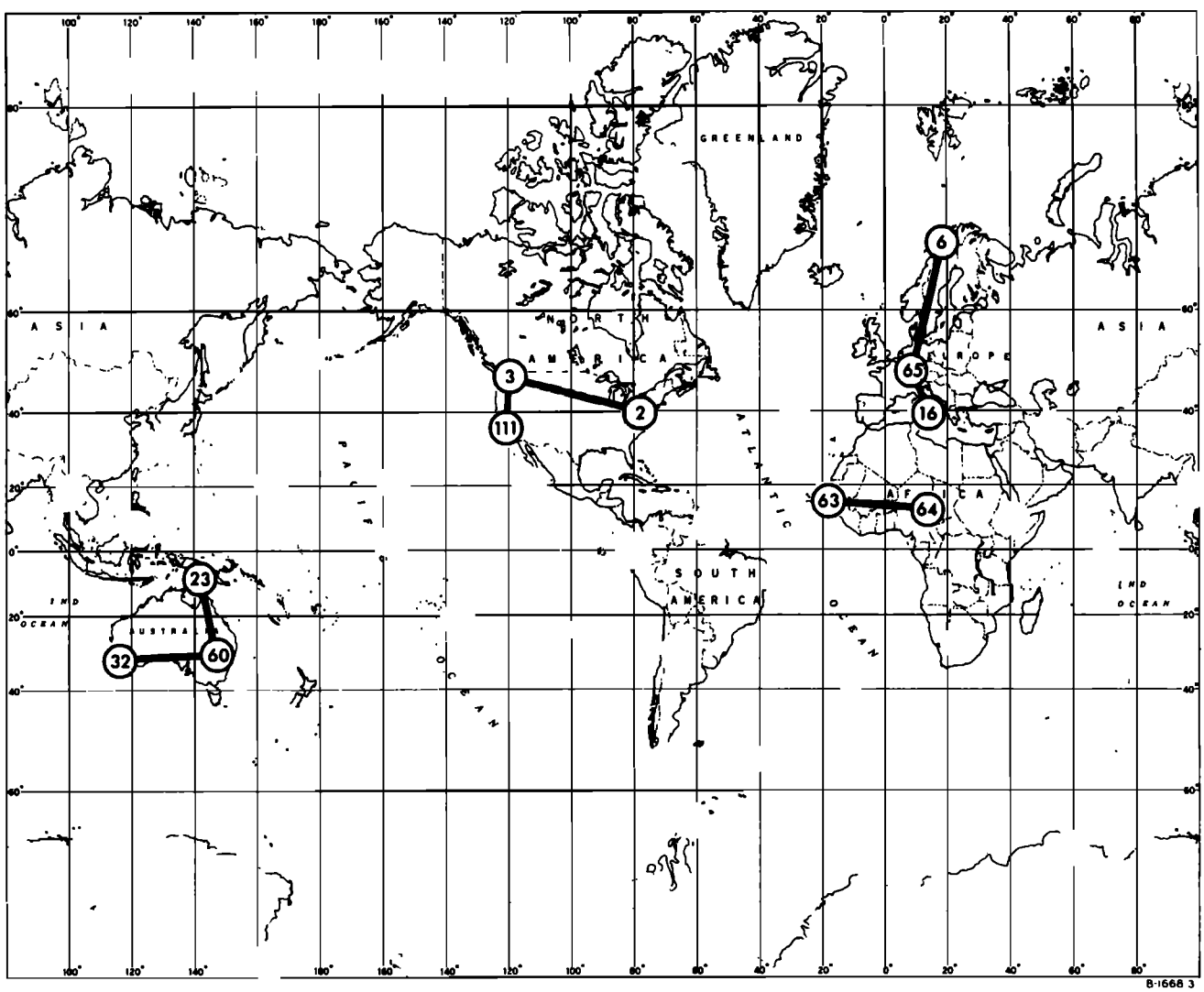

Fig. 4. Scalars connecting observing stations actually measured in the world net program.

A. Observational phase

1. Elimination of possible static instability of the camera during the average half-hour period of observation
2. Elimination of systematic errors in recording the instant of shutter operation that is needed to within a few milliseconds of universal time and relative to all involved cameras to within 1/10 ms

B. Measurement phase

1. Strict adherence to the Abbe comparator principle
2. Correction for the lack of perpendicularity of the comparator axes
3. Accounting for at least linear differences in the comparator scales

C. Adjustment phase

1. Determination of the elements of interior orientation existing in the operational environment
2. Determination of the comparator constants outlined in error sources 2 and 3 of the measurement phase
3. Modeling of astronomic and parallactic refraction, the latter because of the finite distance of the satellite
4. Modeling the phase angle of the satellite illumination as a function of size and shape of the satellite, its reflective property, and the geometric positions of the sun, satellite, and observing station during the event
5. Considering influence of light travel time on station synchronization and aberration
6. Introducing with sufficient accuracy the spatial orientation of the instantaneous rotation axis of the earth (pole wandering) with respect to individual camera orientations as well as with respect to the use of UT1 (true angle of earth's rotation)
7. Reduction of star places to time of observation, involving precession, nutation, proper motion, radial velocity, and annual and diurnal aberration as well as the influence of the spectral characteristics and magnitude of the star on the photogrammetric imagery.

Quantitative results will now be given with respect to the above mentioned random errors and their propagation into the end results of the spatial satellite triangulation, errors in time determination, as previously mentioned, being considered negligible.

Accuracy of the comparator measurements. We discuss first of all the result of measuring 1210 photograms, representing practically half of the observational data from the world net. On each photogram, on the average, 100 fixed stars were recorded before and after the satellite transit and also during the event. With repeated exposure, 500–800 star images in all are thus registered. There are in addition about 300 satellite images, so that on each photogram at least 800 images must be measured. In order to complete these measurements in the time alloted to the world net program, six comparators of similar design were in operation. Of significance also is the fact that a group of operators is involved in the measurements. Each photogram is measured on the comparator in two positions differing by approximately 180°. By means of a two-component translation, two scale factors and a rotation, the two sets of measurements are brought into coincidence by an adjustment. The internal accuracy of the measuring process (precision of the comparator measurements) can then be judged on the basis of residual differences from double measurements. From the selected photograms with their 1,291,744 double measurements there resulted a mean error for the arithmetic mean of a double measurement of ± 1.63 μm. No significant differences between the precisions of the x and y coordinates were detected.

It is of interest to group the measurement of plates by individual operators. The separately computed average measuring accuracy for each of the 34 comparator operators, arranged in sequence of increasing absolute amounts, is shown in Figure 5. The number at the top of each arrow represents the number of photograms measured by the operator, and the ordinates of the arrow heads indicate the range over which the mean errors of the individual plate measurements vary for that operator.

It can be seen that the mean measuring precision attained ranges from ± 1.1 μm (for operator 38) to ± 2.2 μm (for operator 4). The best single result was ± 0.76 μm by operator 38, and the worst was ± 2.66 μm by operator 20. As an explanation of these fairly surprising differences one must assume chiefly the vary-

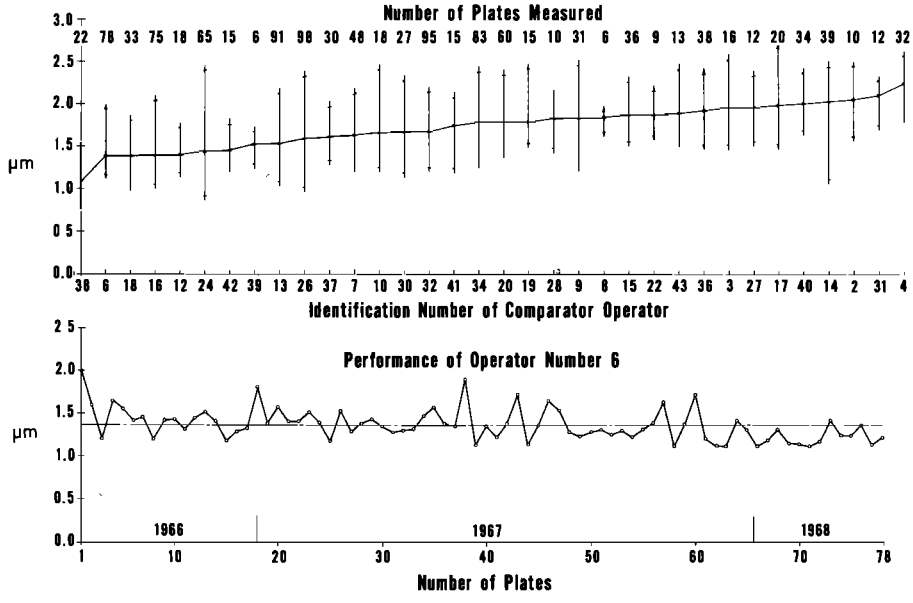

Fig. 5. Comparison of the measuring accuracies attained by a group of comparator operators and the individual performance of one.

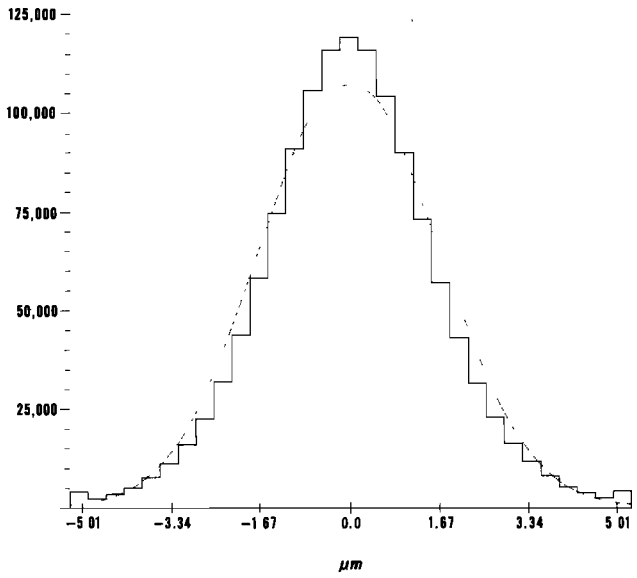

Fig. 6. Histogram of 1,291,744 double measurement differences.

ing capabilities of the operators but also the influence of environmental conditions in image quality. The lower diagram in Figure 5 shows for operator 6 in chronological order the mean error of the 78 photograms measured by him over a period of 18 months. Although the average mean error of this operator of ± 1.37 μm is relatively low, the dispersion is typical for the behavior of all operators with respect to the quality of their individual measuring results. In addition to displaying the variation in precision from plate to plate the diagram indicates a steady though small improvement in the measuring operation.

Figure 6 shows the histogram of the 1,291,744 double measurements. From the similarity of the histogram with the superimposed theoretical normal distribution one can conclude a sufficiently close absence of bias errors, all the more so if one takes into consideration the fact that the data for the histogram are composed of samples with differing mean errors. On the basis of these results one can well imagine that these measurements were all made by one fictitious operator on one fictitious comparator instead of by 34 operators on six comparators. Hence for the further error theoretical studies we shall assume that the internal accuracy of image coordinates, determined as the mean from double measurement, is sufficiently well expressed in their totality by a mean error of ± 1.63 μm. The mean errors m_l, computed separately for each photogram, are plotted in Figure 7 for 500 photograms selected for further study. The observational data selected are derived from 35 stations of the world net plotted according to latitude.

Accuracy of the reconstructions of the photogrammetric bundles and their orientations. The parameters for reconstructing the bundle and its orientation are obtained by relating the measured star image coordinates to the corresponding star catalog data with an adjustment to a mathematical model. The total of these quantities, previously designated as interpolation parameters, includes in addition to the purely photogrammetric parameters a second scale factor and an angle to correct for the a priori assumed perpendicularity of the comparator spindles. The introduction of these extra parameters is justified insofar as one may assume that the homogeneity of the scale of the astronomic reference system (unit sphere) and the orthogonality of its coordinates are superior with respect to systematic errors to the corresponding mechanical components of the comparators. After the linear scale difference between the x and y spindles (periodic screw errors are independently tested for in comparator calibrations) and the deviation from perpendicularity have been determined in this manner, the mean error of ± 1.63 μm computed as a measure of precision for the image coordinates can be considered to be a measure of accuracy for the subsequent treatment. If we assume that the mean error is $\pm 0.3''$ for the astronomic coordinates α, δ of FK-4 stars reduced to the observation datum and $\pm 0.4''$ for all other stars and that the mathematical model for simulation of the bundle is sufficient, then since time errors are negligible, the mean error of coordinate corrections resulting from an adjustment executed with appropriate weights will express the additive influence of the random errors produced by the comparator measurement, scintillation, and emulsion shift. In Figure 7 are listed for the 500 selected photograms the values for m_p and m_l and the rms for all the data, m_p being the mean error of the image coordinates for the photogram as obtained from the adjustment for the photogrammetric bundle reconstruction and m_l being the expression for the accuracy of the corresponding comparator measurements. A mean error of ± 1.0 μm is assumed for the influence of random emulsion shift [*Altman and Ball,* 1961]. Hence the contribution to the total mean error m_p by the scintillation is

$$m_s = \pm(m_p^2 - m_l^2 - 1.0^2)^{1/2} \qquad (1)$$

This error component is also listed in Figure 7. The rms values for the 500 plates are

$$m_p = \pm 3.31\ \mu\text{m} \qquad m_l = \pm 1.81\ \mu\text{m} \qquad m_s = \pm 2.58\ \mu\text{m}$$

Figure 8 shows the histogram of combined x and y coordinate corrections with corresponding normal distribution curves for five single-camera adjustments. These were selected to cover uniformly the range of mean coordinate errors after adjustment actually obtained. The histograms illustrate the typical behavior of the totality of evaluated observational data.

Accuracy of the trace of the satellite orbit after the polynomial fit. The mean deviation of a measured satellite point from the smoothing polynomial of degree 6 varies between ± 1.6 μm and ± 8.6 μm with an rms of ± 3.75 μm for the fit in direction of the satellite trail and between ± 1.3 μm and ± 9.3 μm with an rms of ± 3.28 μm perpendicular to the trail (cf. Figure 9). The corresponding x, y mean value is ± 3.52 μm.

The individual mean displacement is a measure of how well the satellite images on a given photogram fit the polynomial. These quantities are the sums of the superimposed random errors of the comparator measurements, the emulsion shifts, and again the scintillation. The mean deviation in direction of the satellite trail is on the average 0.47 μm larger than that at right angles to the trail. This is not so much due to random time errors of the recording sequence that operate in the direction of the trail as it is to the fact that the comparator measurements of the trail images have a larger mean error in this direction than in the direction perpendicular to the trail because of image blur from the satellite motion.

About 300 satellite image measurements are available per plate. From the double measurements and their differences the accuracy of the comparator measurements is again determined. This is on the average ± 1.79 μm for the x and y measurements, or practically the same value as for the star image measurements. Again, with the assumption of ± 1.0 μm for the mean random emulsion shift the opportunity is given to

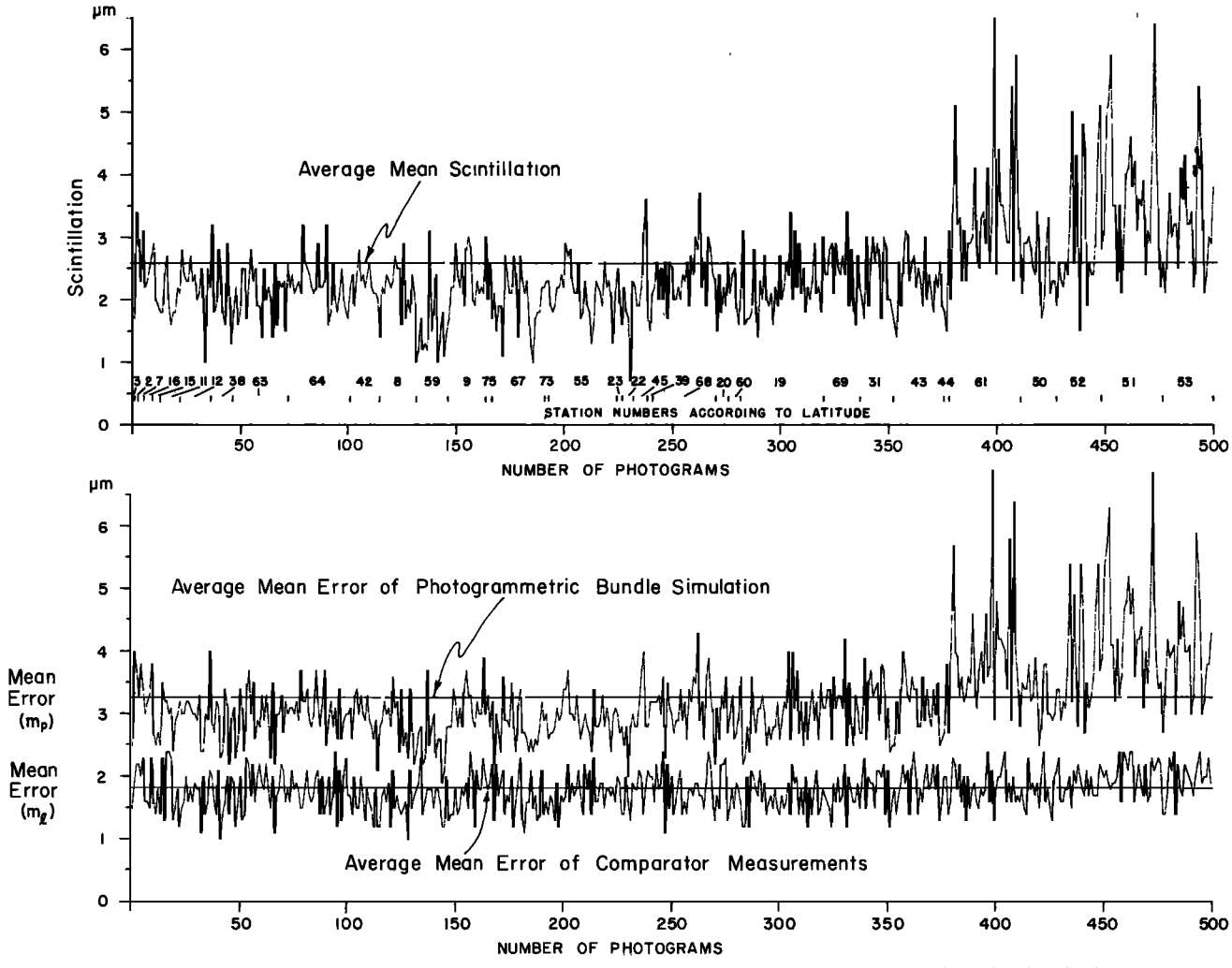

Fig. 7. Five hundred photograms, arranged according to increasing latitude of observing station, showing, in the top diagram, the amount of scintillation for each plate and, below, the mean errors of the bundle simulation and the comparator measurements, respectively.

isolate the scintillation effect as

$$m_s = (3.52^2 - 1.79^2 - 1.0^2)^{1/2} = \pm 2.86\ \mu\text{m} \qquad (2)$$

The treatment of the scintillation as a random source of error is based on the fact known from astronomical observations [*Hynek,* 1960] that the mean amplitude of scintillation operates as an irregular error source in all directions. By computing for each plate the scintillation effect on the star images in accordance with (1) and comparing these values with the corresponding similar values obtained from the curve fit with (2), the correlation coefficient $\rho = 0.81 \pm 0.02$ is obtained with the formula

$$\rho = \frac{\sum_{i=1}^{n=500} \Delta s_1 \cdot \Delta s_2}{\left[\sum_{i=1}^{n=500} \Delta s_1^{\,2}\right]^{1/2} \left[\sum_{i=1}^{n=500} \Delta s_2^{\,2}\right]^{1/2}} \qquad (3)$$

where the Δ represent deviations of the individual amounts of scintillation from their mean value and the indices 1 and 2 refer, respectively, to the scintillation computed from the bundle reconstructions and from the polynomial fit.

In Figure 10 is shown the mean scintillation at each observing station, the stations being arranged by latitude. From this it is seen that scintillation, with an overall mean for all stations of $\pm 2.58\ \mu$m for the star images and $\pm 2.86\ \mu$m for satellite images, represents a considerable error contribution to the total error budget. Also apparent is the increase in scintillation with increasing latitude, which is to be expected in consequence of the theory presented by *Nettelblad* [1953], according to which scintillation is least in warm ocean air masses and greatest in cold continental climates. The amplitude of the scintillation depends, in addition, on the exposure time, which may be the cause for the fact that the mean scintillation for the star exposures of between 0.2 and 3.2 s is $\pm 2.58\ \mu$m and for the

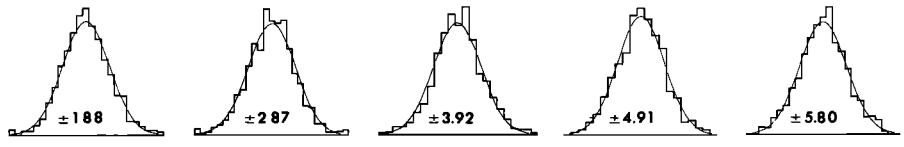

Fig. 8. Histograms of x and y plate residuals for five typical single-camera adjustments, with mean coordinate errors in micrometers.

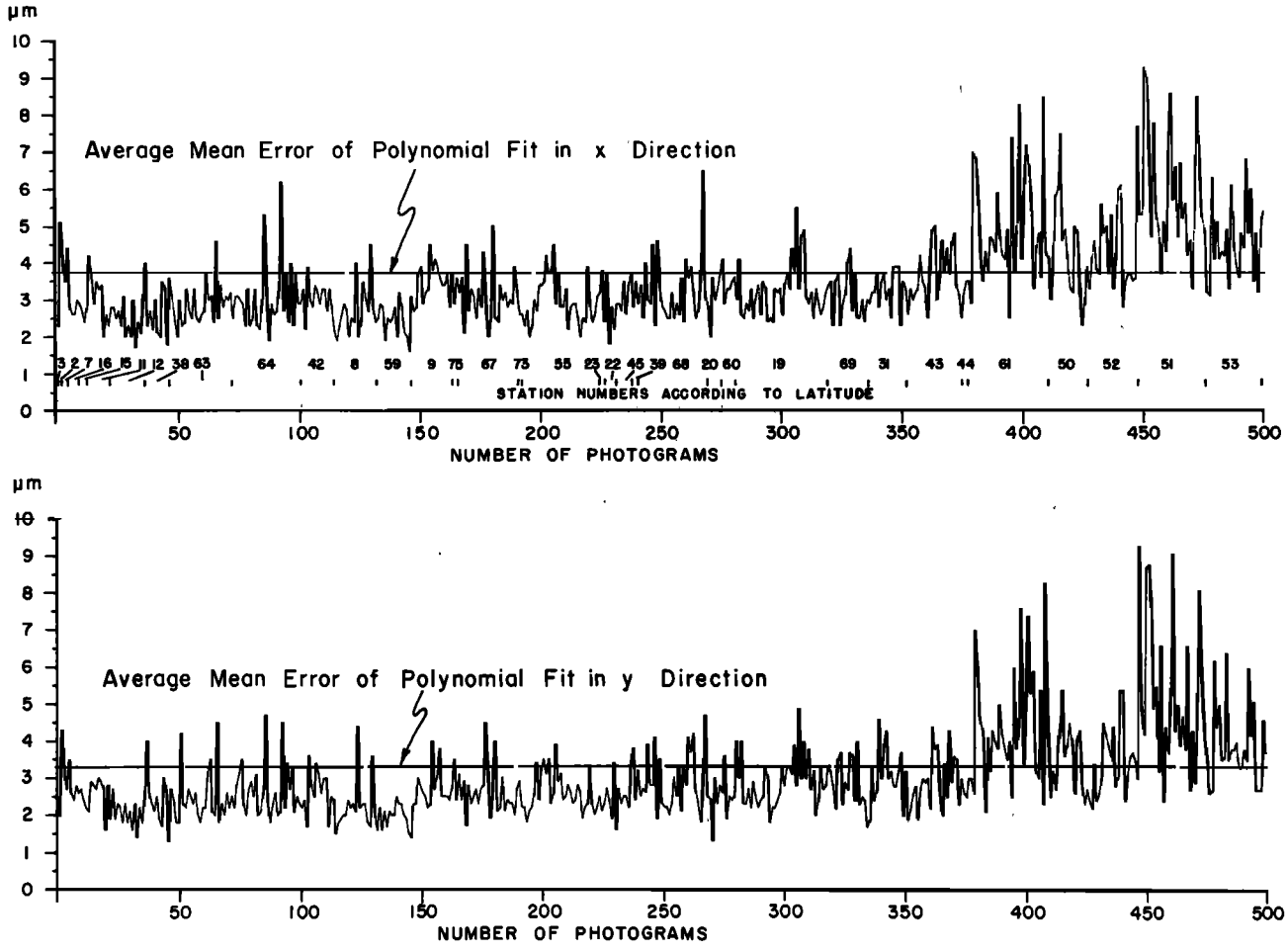

Fig. 9. Plot of the mean errors of the individual polynomial fits to the satellite trail for each of the 500 plates of Figure 7. The top diagram refers to the polynomials fitted to displacements in direction of the trail, and the bottom one to the fits perpendicular to the trail.

satellite images exposed from 1/15 to 1/30 s is ±2.86 μm. Obviously, the use of short-duration flashes (1/1000 s) will increase the scintillation effect for the individual flash, this effect thus making it all the more desirable to have a considerable number of such flashes before an adequately accurate triangulation can be performed.

Error propagation into the spatial triangulation. In the three preceding sections on accuracy, quantitative results have been given for the significant random error contributions that must be considered in setting up an error budget for spatial triangulation. In Table 2, average values from the processing of the selected 500 photograms are presented.

The figure in column 7 of Table 2 indicates that an average uncertainty of 1.57″ in direction should be associated with a

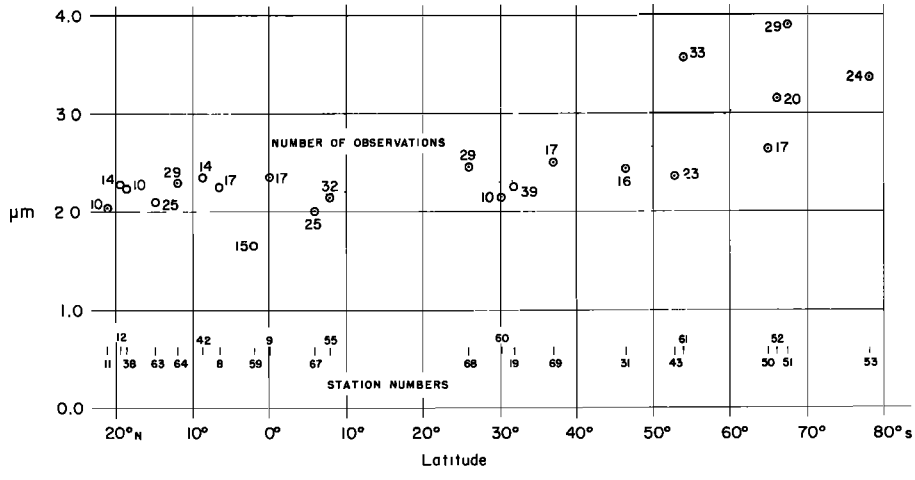

Fig. 10. Average scintillation at a number of observing stations arranged according to latitude, showing a corresponding trend curve.

bundle reconstruction that is not overdetermined. Actually, this value is a function of the position of a ray within this bundle [*Schmid*, 1967] and to be completely rigorous, in accordance with error theory, should be computed with the covariance matrix obtained from the individual bundle reconstruction adjustment. However, since the bundles under consideration here are relatively narrow (the angle of vision for the BC-4 camera is about 20°), we can for the present ignore this fact in a general examination of the error propagation. In order to determine uniquely the 20 required interpolation parameters of an oriented bundle reconstruction, at least 10 reference stars are required, so that the use of an average of 100 stars per plate represents 10 solutions in the adjustment. Each star being measured on the average 5 times, from a combination of tabulated values in Table 2 it can be expected that the direction uncertainty for a central ray after adjustment of the bundle reconstruction will be as follows:

The error sources affecting the individual image coordinates add quadratically to

$$m_i = \pm(1.81^2 + 1.0^2 + 2.58^2)^{1/2} = \pm 3.31\ \mu\text{m}$$

(cf. Table 2, columns 2, 3, 4, and 5). If we assume that the five images for each reference star combine into one fictitious image, then the coordinates will have an accuracy of $3.31/(5)^{1/2} = \pm 1.48\ \mu$m. When it is combined with the mean star catalog uncertainty of $\pm 0.4'' = \pm 0.87\ \mu$m (column 6), we have a mean uncertainty in the direction of $\pm 1.72\ \mu\text{m} = \pm 0.79''$. The combination of 10 independent solutions in one adjustment reduces this error approximately to $0.79''/(10)^{1/2} = 0.25''$.

The figures of Table 3 are results from a bundle reconstruction adjustment with a mean error of $\pm 3.31\ \mu$m for the image coordinates after adjustment involving 648 star images of 105 reference stars distributed approximately evenly over the plate. The results shown are mean accuracies of directions corresponding to various image positions on the plate assumed to be free of error.

The mean error $\pm 0.23''$ from this table for the central ray ($x = y = 0$) is in good agreement with the value $0.25''$ obtained before from general considerations. With the use of the mean satellite image error figure of $1.61''$ from Table 2, column 8, the sixth-degree polynomial fit over 300 satellite points will contribute an uncertainty in direction after adjustment of $\pm 1.61''/(300/7)^{1/2} = 0.25''$. The error sources being uncorrelated, the total expected error in direction for the central ray is $[(0.25'')^2 + (0.25'')^2]^{1/2} = \pm 0.35''$.

The use of sixth-degree polynomials makes seven directions available for satellite triangulation in each photographed bundle. However, as we know, these are mutually correlated. One reason is that they are all obtained with a specific group of interpolation parameters from one single camera, and for another they all derive from a single pair of smoothing polynomials. From a study of the relevant covariance matrices in a rigorous adjustment whose reproduction here would far exceed the available space, it becomes apparent that the use of seven directions distributed evenly over the satellite trail yields a gain of 32% for the geometry of the bundles as opposed to the use of a single central direction. This means that the use of all seven directions has about the same information content that would be obtained from two central rays that are not correlated.

Hence if we conceive of the total information used in the evaluation of a specific photogram as being compressed to determine a central fictitious direction, we may expect for such a

TABLE 2. Average Values From the Processing of 500 Selected Photograms

	Type of Imagery (1)	Mean Errors of Comparator Measurements m_η, μm (2)	Assumed Mean of Irregular Emulsion Shift, μm (3)	Average of Mean Scintillation (4)		Mean Coordinate Error,* μm (5)	Introduced Mean Error,† (6)		Total Noise (7)§		Mean Error¶ (8)	
				μm	sec		μm	sec	μm	sec	μm	sec
Average values	stars	±1.81	±1.00	±2.58	±1.18	±3.31	±0.87	±0.40	±3.42	±1.57	...	...
	satellite	±1.79	±1.00	±2.86	±1.31	...	...	...	...	...	±3.52	±1.61
Minimal values	stars	±0.97	±1.00	±1.01	±0.46	±1.88	±0.87	±0.40	±1.93	±0.88	...	...
	satellite	±0.87	±1.00	±1.07	±0.47	...	...	...	...	...	±1.46	±0.67
Maximal values	stars	±2.45	±1.00	±6.46	±2.96	±6.87	±0.87	±0.40	±7.03	±3.22	...	...
	satellite	±2.68	±1.00	±6.84	±3.14	...	...	...	...	...	±8.96	±4.11

Photogrammetric camera was Wild BC-4, lens was Cosmotar $f = 450$ mm, and aperture was 132 mm. The target was Pageos balloon satellite for 496 photograms and Echo satellite for four photograms. The program was world net. The period of observation was October 1966 to September 1969. The observation material consisted of 500 selected photograms with corresponding time recordings from 35 stations in the world net.

*After adjustment in photogrammetric bundle simulation $[(2)^2 + (3)^2 + (4)^2]^{1/2}m_\eta$.

†Of reduced star catalog data.

§In photogrammetric bundle simulation adjustment $[(2)^2 + (3)^2 + (4)^2 + (6)^2]^{1/2}$.

¶Of polynomial smoothing $[(2)^2 + (3)^2 + (4)^2]^{1/2}$.

bundle reconstruction that is not overdetermined. Actually, this value is a function of the position of a ray within this bundle [*Schmid*, 1967] and to be completely rigorous, in accordance with error theory, should be computed with the covariance matrix obtained from the individual bundle reconstruction adjustment. However, since the bundles under consideration here are relatively narrow (the angle of vision for the BC-4 camera is about 20°), we can for the present ignore this fact in a general examination of the error propagation. In order to determine uniquely the 20 required interpolation parameters of an oriented bundle reconstruction, at least 10 reference stars are required, so that the use of an average of 100 stars per plate represents 10 solutions in the adjustment. Each star being measured on the average 5 times, from a combination of tabulated values in Table 2 it can be expected that the direction uncertainty for a central ray after adjustment of the bundle reconstruction will be as follows:

The error sources affecting the individual image coordinates add quadratically to

$$m_i = \pm(1.81^2 + 1.0^2 + 2.58^2)^{1/2} = \pm 3.31\ \mu\text{m}$$

(cf. Table 2, columns 2, 3, 4, and 5). If we assume that the five images for each reference star combine into one fictitious image, then the coordinates will have an accuracy of $3.31/(5)^{1/2} = \pm 1.48\ \mu$m. When it is combined with the mean star catalog uncertainty of $\pm 0.4'' = \pm 0.87\ \mu$m (column 6), we have a mean uncertainty in the direction of $\pm 1.72\ \mu\text{m} = \pm 0.79''$. The combination of 10 independent solutions in one adjustment reduces this error approximately to $0.79''/(10)^{1/2} = 0.25''$.

The figures of Table 3 are results from a bundle reconstruction adjustment with a mean error of $\pm 3.31\ \mu$m for the image coordinates after adjustment involving 648 star images of 105 reference stars distributed approximately evenly over the plate. The results shown are mean accuracies of directions corresponding to various image positions on the plate assumed to be free of error.

The mean error $\pm 0.23''$ from this table for the central ray ($x = y = 0$) is in good agreement with the value $0.25''$ obtained before from general considerations. With the use of the mean satellite image error figure of $1.61''$ from Table 2, column 8, the sixth-degree polynomial fit over 300 satellite points will contribute an uncertainty in direction after adjustment of $\pm 1.61''/(300/7)^{1/2} = 0.25''$. The error sources being uncorrelated, the total expected error in direction for the central ray is $[(0.25'')^2 + (0.25'')^2]^{1/2} = \pm 0.35''$.

The use of sixth-degree polynomials makes seven directions available for satellite triangulation in each photographed bundle. However, as we know, these are mutually correlated. One reason is that they are all obtained with a specific group of interpolation parameters from one single camera, and for another they all derive from a single pair of smoothing polynomials. From a study of the relevant covariance matrices in a rigorous adjustment whose reproduction here would far exceed the available space, it becomes apparent that the use of seven directions distributed evenly over the satellite trail yields a gain of 32% for the geometry of the bundles as opposed to the use of a single central direction. This means that the use of all seven directions has about the same information content that would be obtained from two central rays that are not correlated.

Hence if we conceive of the total information used in the evaluation of a specific photogram as being compressed to determine a central fictitious direction, we may expect for such a

TABLE 2. Average Values From the Processing of 500 Selected Photograms

	Type of Imagery (1)	Mean Errors of Comparator Measurements m_η, μm (2)	Assumed Mean of Irregular Emulsion Shift, μm (3)	Average of Mean Scintillation (4)		Mean Coordinate Error,* μm (5)	Introduced Mean Error,† (6)		Total Noise (7)§		Mean Error¶ (8)	
				μm	sec		μm	sec	μm	sec	μm	sec
Average values	stars	±1.81	±1.00	±2.58	±1.18	±3.31	±0.87	±0.40	±3.42	±1.57	...	...
	satellite	±1.79	±1.00	±2.86	±1.31	...	...	...	...	...	±3.52	±1.61
Minimal values	stars	±0.97	±1.00	±1.01	±0.46	±1.88	±0.87	±0.40	±1.93	±0.88	...	...
	satellite	±0.87	±1.00	±1.07	±0.47	...	...	...	...	...	±1.46	±0.67
Maximal values	stars	±2.45	±1.00	±6.46	±2.96	±6.87	±0.87	±0.40	±7.03	±3.22	...	...
	satellite	±2.68	±1.00	±6.84	±3.14	...	...	...	...	...	±8.96	±4.11

Photogrammetric camera was Wild BC-4, lens was Cosmotar $f = 450$ mm, and aperture was 132 mm. The target was Pageos balloon satellite for 496 photograms and Echo satellite for four photograms. The program was world net. The period of observation was October 1966 to September 1969. The observation material consisted of 500 selected photograms with corresponding time recordings from 35 stations in the world net.

*After adjustment in photogrammetric bundle simulation $[(2)^2 + (3)^2 + (4)^2]^{1/2} m_\eta$.

†Of reduced star catalog data.

§In photogrammetric bundle simulation adjustment $[(2)^2 + (3)^2 + (4)^2 + (6)^2]^{1/2}$.

¶Of polynomial smoothing $[(2)^2 + (3)^2 + (4)^2]^{1/2}$.

TABLE 3. Mean Accuracies of Directions

Image coordinates x/y, mm	0/0	10/10	20/20	30/30	40/40	50/50	60/60	70/70
Mean accuracy of direction	±0.23"	±0.25"	±0.19"	±0.21"	±0.21"	±0.25"	±0.44"	±2.77"

direction an accuracy of $m_r = \pm 0.35'' - 32\%(\pm 0.35'') = 0.24''$.

According to the section on the method of geometric satellite triangulation the adjustment algorithm is based on the assumption that the results of bundle reconstructions at the individual stations are uncorrelated. Consequently, the directions to the satellite for a given event derived at the individual stations are likewise uncorrelated. To obtain a measure of the mean accuracy to be expected for the spatial triangulation of the observing sites, one can therefore assume that the mean accuracy 0.24" of a direction computed above for a fictitious central direction containing all the information content is an uncorrelated function of the station. In the adjustment algorithm this accuracy of triangulation directions associated with a specific evaluation of a photogram is expressed in the form of the weight matrix associated with the coordinates of the seven fictitious satellite images, the weight matrix being computed from the corresponding covariance matrix. In the section on the method of geometric satellite triangulation it was mentioned that in the mathematical formulation to be set up for the final triangulation, only the satellite and station positions were to be determined as unknowns. From the basic triangulation geometry it is then obvious that the accuracy of the triangulation results to be expected in a direction perpendicular to the station-satellite direction is proportional both to the directional accuracy and the distance between the station and the satellite. This is indicated schematically and reduced to two dimensions in Figure 11.

The accuracy in direction of the z coordinate is obviously a function of the angle γ in which the station-satellite planes intersect. From analysis of the inverted normal equation systems, which contain the geometry of the actual satellite observations, it follows quite generally that the mean error of the triangulated station in direction of the geodetic latitude and longitude is, if the scale is errorless, proportional to the product $m_R \cdot d$, where m_R is the mean error of direction and d the mean station-satellite distance; on the other hand, the average mean error in the direction of height is 3 times as large [*Schmid*, 1967]. These relations are shown in Figure 12, in which $Q^{1/2}$ is the error propagation factor (sometimes called the weight reciprocal) for the position coordinate.

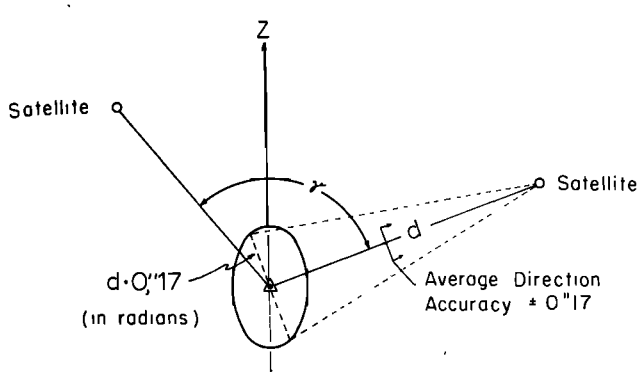

Fig. 11. Section of error ellipsoid at observation station intersected from two satellite positions.

The same result is shown schematically in another form in Figure 13, from which by comparison of antipodal stations it is apparent that the uncertainty in height determination within a world triangulation eventually has the effect of an uncertainty in scale. One can expect therefore that additional scale control will have particularly favorable influence on the accuracy of height coordinates but will represent no real gain for the determination of the position coordinates φ, λ. This fact is illustrated in Figure 12, showing the effect of from one to four scale determinations. The lower part of Figure 12 shows that even under the assumption of errorless scalars (weight 10^4), only the stations directly involved in the scale determinations show a gain in the determination of their latitude φ and longitude λ. On the other hand, the error propagation coefficient for the height determination reduces from 3 to 1.8 with the use of four scalars even when a more realistic weight of 1 is used in the scale determination [*Schmid*, 1967; *Rinner*, 1966].

In the world net the Pageos satellite was observed almost exclusively. Its nominal circular orbit elevated about 4600 km above the surface of the earth resulted in an average station-satellite distance of 6000 km. With a mean direction accuracy of 0.24" and the propagation factors of Figure 12 a triangulation solution based on two satellite transits or events per triangle side, if the scale is errorless, produces position coordinates for the observing stations with mean errors $m_\varphi = m_\lambda = \pm 7.0$ m and $m_H = \pm 21.0$ m. At this time, 2350 plates have been reduced for evaluation in the world net. These observations correspond to about five independent solutions. An adjustment of all these events should therefore yield an accuracy of $m_\varphi = m_\lambda = \pm 7.0/(5)^{1/2} = \pm 3.1$ m and $m_H = \pm 21.0/(5)^{1/2} = \pm 9.4$ m. With the introduction of the planned four scalars, measured independently and with an accuracy of at least 1:1,000,000, the expected mean error in height reduces to $m_H = \pm 3.1$ m $\times$ 1.8 $= \pm 5.6$ m (cf. Figure 12), and the mean position error of a station

$$M = \pm\left(\frac{m_\varphi^2 + m_\lambda^2 + m_H^2}{3}\right)^{1/2} = \pm 4.1 \text{ m} \quad (4)$$

or M is roughly 1:1,500,000 of the mean station-satellite distance.

In the following paragraphs the result of the worldwide geometric satellite triangulation program is presented with an associated error analysis based on the statistical information obtained during the final triangulation adjustment.

Result of the Worldwide Geometric Satellite Triangulation

The quantitated result of the worldwide geometric satellite triangulation program consists of the three-dimensional positions of 45 stations. Their locations can be seen from Figure 14.

The corresponding Cartesian reference coordinate system has one of its axes parallel to the rotation axis of the earth for a

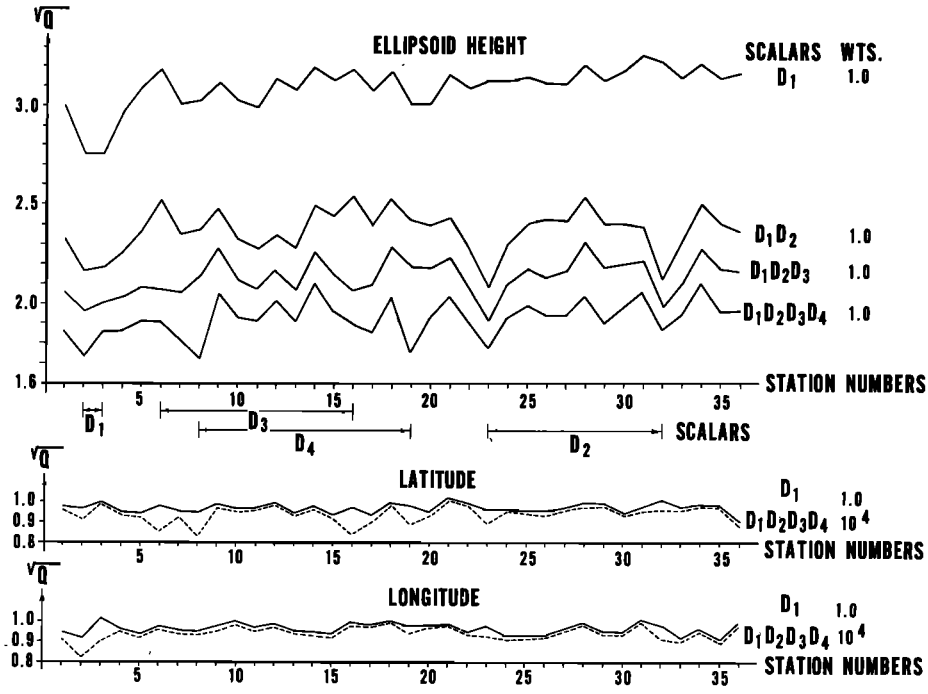

Fig. 12. Error propagation factors for ellipsoid height, latitude, and longitude using from one to four scalars.

certain epoch (Conventional International Origin). The origin of the system and the selection of the X direction are, for reasons inherent to the method of geometric satellite triangulation, arbitrary. They were fixed by enforcing for station 2, Beltsville, United States, the following spatial coordinates, which are approximation values for a mass-centered position.

$$X = 1130761.500 \text{ m}$$

$$Y = 4830828.597 \text{ m}$$

$$Z = 3994704.584 \text{ m}$$

As is discussed in the analysis of the results in the next paragraph, it was decided to enforce all eight scalars with their measured values.

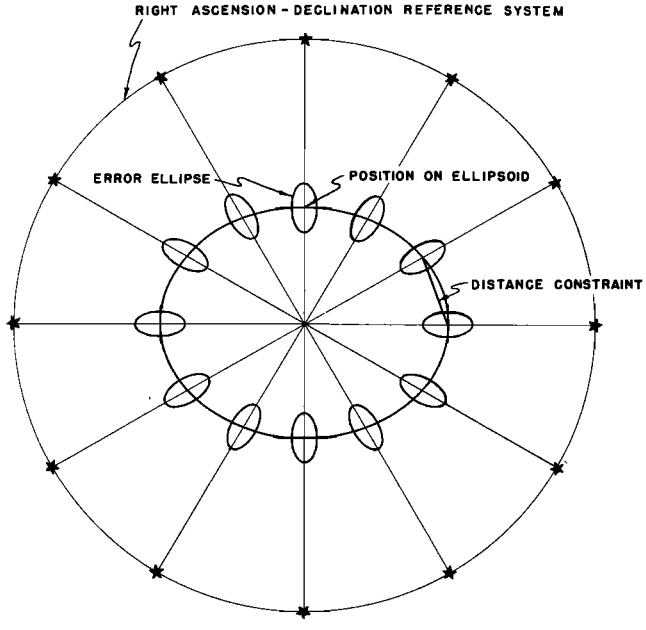

Fig. 13. Error propagation of the method of geometric satellite triangulation.

Table 4 lists the three-dimensional Cartesian coordinates for the 45 stations and their mean errors as obtained from the final adjustment. (The XYZ system is a left-handed system (west longitude positive). The complete covariance matrix for the triangulated station coordinates, which for space reasons cannot be presented here, is available.) The coordinates refer to the projective center of the BC-4 cameras. The elevation of this point above the permanent station mark is in each case +1.5 m.

Analysis of the Triangulation Adjustment

The input of the triangulation adjustment refers to the information obtained from the evaluation of 2350 photographic plates. Specifically, the observations from 856 two-station, 194 three-station, and 14 four-station satellite events were used. The 1064 satellite events chosen for evaluation required, in addition to the determination of the spatial positions of the tracking stations, the triangulation of 6604 satellite positions. The adjustment provided for 9162 degrees of freedom. Two station-to-station couplings were introduced as additional constraints in order to tie together the stations 111 and 134 (California) and 012 and 066 (Wake Island) where for technical reasons, satellite observations were collected from neighboring observation piers. Furthermore, eight scalars were rigorously introduced. They represent the spatial distances between the stations in Table 5.

In order to obtain a measure for the precision of the strictly photogrammetric triangulation a first triangulation adjustment was executed with only the scalar between stations 002 and 003 enforced. This adjustment produced a sum of the squares of the weighted residuals in terms of plate coordinate corrections $[pvv] = (3.064 \pm 0.045) \times 10^{-8}$ (m^2).

A comparison of the measured base lines with the corresponding triangulation results provides a first insight into the internal accuracy of the geometric world net. The

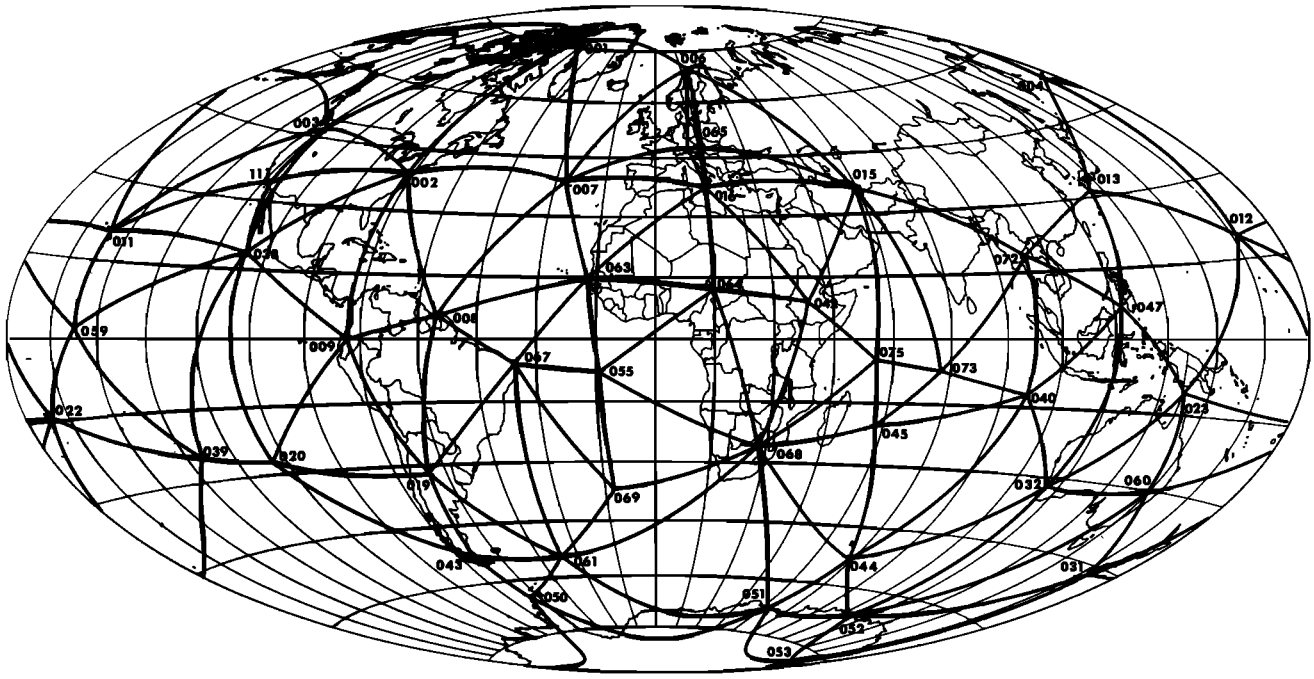

Fig. 14. The 45 stations of the worldwide BC-4 photogrammetric satellite triangulation network with station number designations.

TABLE 4. Three-Dimensional Cartesian Coordinates

Station No. and Name	X, m	σ_X, m	Y, m	σ_Y, m	Z, m	σ_Z, m
1, Thule	546567.862	±2.297	1389990.609	±3.447	6180239.602	±3.960
2, Beltsville	1130761.500	0	4830828.597	0	3994704.584	0
3, Moses Lake	-2127833.613	±0.790	3785861.054	±2.976	4656034.740	±2.906
4, Shemya	-3851782.861	±4.888	-396404.016	±5.654	5051347.586	±6.673
6, Tromso	2102925.118	±3.663	-721667.562	±4.772	5958188.868	±4.748
7, Azores	4433636.070	±4.737	2268143.467	±4.362	3971656.223	±4.945
8, Surinam	3623227.823	±4.563	5214231.698	±4.502	601551.302	±5.716
9, Quito	1280815.597	±4.338	6250955.436	±5.800	-10793.013	±5.717
11, Maui	-5466020.732	±5.045	2404435.198	±4.352	2242229.885	±4.703
12, Wake	-5858543.398	±5.308	-1394489.166	±5.281	2093807.584	±5.391
13, Kanoya	-3565865.509	±5.200	-4120692.866	±6.694	3303428.249	±6.131
15, Mashhad	2604346.389	±3.988	-4444141.147	±5.513	3750323.381	±4.974
16, Catania	4896383.234	±4.080	-1316167.822	±4.463	3856673.791	±4.698
19, Dolores	2280603.832	±4.190	4914545.588	±4.789	-3355412.286	±6.839
20, Easter	-1888616.886	±4.845	5354892.780	±6.246	-2895739.444	±7.217
22, Pago Pago	-6099954.446	±5.392	997367.321	±4.710	-1568567.088	±5.883
23, Thursday Isl.	-4955371.694	±4.671	-3842221.799	±5.689	-1163828.451	±5.852
31, Invercargill	-4313815.856	±4.687	-891322.098	±5.238	-4597238.676	±6.398
32, Perth	-2375397.874	±4.579	-4875524.035	±5.746	-3345372.936	±6.170
38, Revilla	-2160983.561	±2.008	5642711.612	±3.653	2035371.417	±4.062
39, Pitcairn	-3724766.403	±6.502	4421236.249	±6.480	-2686072.609	±7.288
40, Cocos	-741969.205	±4.859	-6190770.789	±6.606	-1338530.638	±5.843
42, Addis Ababa	4900734.926	±4.844	-3968226.427	±5.481	966347.675	±5.103
43, Sombrero	1371358.188	±4.171	3614760.271	±4.969	-5055928.396	±8.156
44, Heard	1098896.432	±6.448	-3684591.597	±7.801	-5071838.356	±9.919
45, Mauritius	3223422.870	±4.472	-5045312.452	±6.019	-2191780.736	±6.065
47, Zamboanga	-3361946.845	±4.909	-5365778.338	±6.501	763644.128	±6.121
50, Palmer	1192659.730	±5.174	2450995.361	±7.275	-5747040.896	±10.171
51, Mawson	1111335.585	±5.189	-2169243.189	±5.456	-5874307.692	±8.002
52, Wilkes	-902598.435	±4.912	-2409507.607	±5.700	-5816527.805	±7.901
53, McMurdo	-1310841.759	±4.993	-311248.105	±5.500	-6213251.231	±7.886
55, Ascension	6118325.238	±5.260	1571746.070	±4.816	-878595.457	±5.507
59, Christmas	-5885331.078	±5.213	2448376.867	±4.435	221683.837	±5.446
60, Culgoora	-4751637.577	±4.552	-2792039.266	±5.653	-3200142.319	±5.866
61, S. Georgia	2999903.036	±4.896	2219368.228	±6.055	-5155246.454	±8.547
63, Dakar	5884457.561	±4.898	1853492.773	±4.257	1612863.206	±5.072
64, Chad	6023375.533	±4.690	-1617924.383	±4.242	1331742.422	±4.834
65, Hohenpeissenberg	4213552.554	±3.730	-820823.968	±4.444	4702787.513	±4.620
67, Natal	5186398.560	±5.260	3653936.203	±4.854	-654277.651	±5.569
68, Johannesburg	5084812.984	±5.229	-2670319.559	±5.065	-2768065.639	±6.586
69, De Cunha	4978412.958	±8.167	1086867.619	±6.918	-3823159.761	±9.443
72, Thailand	-941692.348	±5.593	-5967416.884	±6.919	2039317.530	±5.461
73, Chagos	1905130.320	±4.345	-6032252.624	±6.702	-810711.562	±5.751
75, Mahé	3602810.169	±4.910	-5238217.287	±6.393	-515928.653	±5.650
111, Wrightwood	-2448854.721	±2.088	4667988.213	±3.367	3582758.969	±3.185

TABLE 5. Directly Measured Distance Constraints

Stations Between Which Scalars Were Measured	Spatial Distances, m	σ_d, m
002-003	3,485,363.232	±3.53
003-111	1,425,876.452	±1.59
006-065	2,457,765.810	±0.80
065-016	1,194,793.601	±1.43
006-016*	3,545,871.454	±1.64
023-060	2,300,209.803	±0.88
032-060	3,163,623.866	±0.98
063-064	3,485,550.755	±2.10

*The scalar 006-016 is not a truly independent scalar.

TABLE 6. Corrections to Base Lines in Adjustment

Scalar	Δd,* m	σ of Scalar,† m
002-003	0	0 (held fixed)
003-111	-7.3	±2.8
006-065	-2.0§	±4.9
065-016	+9.3	±5.1
023-060	+5.8	±3.9
032-060	+8.5	±4.6
063-064	-5.1	±5.2
Sum	+9.16	±15.61¶

*Δd equals measured distance minus computed distance.
†As obtained from the triangulation adjustment.
§The German Geodetic Research Institute gives for the base line 006-065 a value that is 1.9 m larger than the one used here. The corresponding Δ values would then be only 1 dm.
¶σ of Σd.

TABLE 7. Corrections to Scalars

Scalar	Assumed Mean Error, m	Correction From the Adjustment, m
002-003	±1.75	-0.06
003-111	±0.72	+1.50
006-016	±1.78	-0.26
006-065	±1.23	0.10
016-065	±0.60	0.42
023-060	±1.15	-0.98
032-060	±1.58	-2.76
063-064	±1.75	+2.60

differences between the computed and measured distances with a complete constraint on scalar 002–003 are shown in Table 6. The sum $\sum d$ of the lengths of the measured scalars is 17,513,184 m, so that

$$\frac{\sum \Delta d}{\sum d} = 1{:}1{,}911{,}920$$

As can be seen from Table 6, the difference $\sum \Delta d$ is only about 0.6 of the standard deviation associated with the sum of the triangulated distances.

It was therefore concluded that the scalars, at least in their totality, are probably of higher accuracy than the geometric satellite triangulation itself, a conclusion that is further evidenced when the standard errors for these scalars computed by the various computing centers are considered.

An adjustment in which all scale lines were enforced with weights corresponding to an accuracy of 1 ppm of their respective lengths gave the following result, as shown in Table 7.

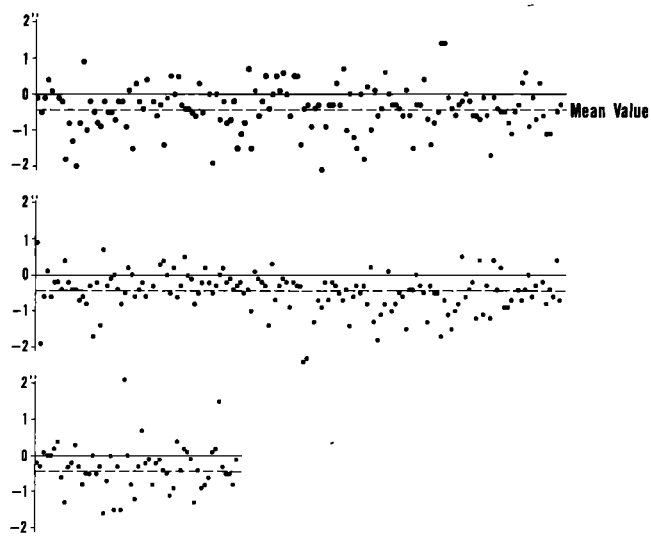

Fig. 15. Plot of the increments in $A \cos E$ from precalibration to post calibration for a number of randomly selected events, in seconds of arc. The three segments are portions of a single graph.

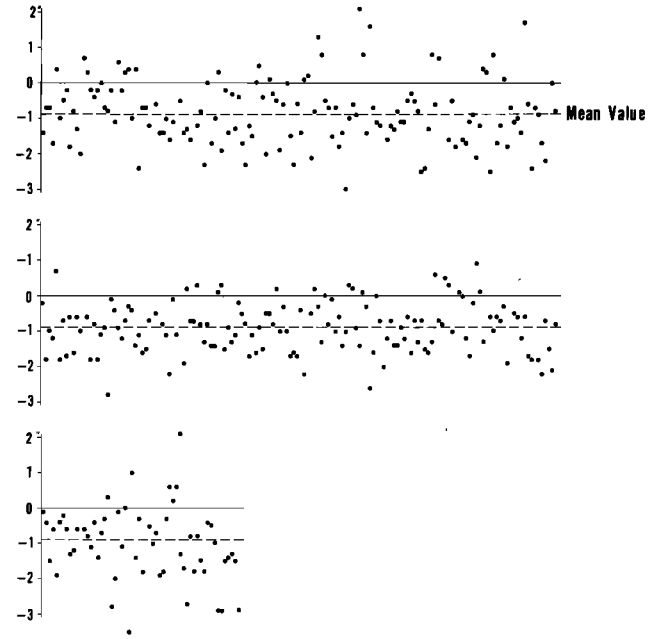

Fig. 16. Plot of the increments in elevation from precalibration to postcalibration for a number of randomly selected events, in seconds of arc. The three segments are portions of a single graph.

The [*pvv*] of this adjustment was 3.068×10^{-8}, or a value which is only 0.004×10^{-8} units larger when it is compared with the single scalar adjustment mentioned above. This difference is only one tenth of the associated sigma. It can therefore safely be concluded that the scalars do not exercise undue constraint on the triangulation system.

If all eight scalars are rigorously enforced, the [*pvv*] sum increases to 3.071×10^{-8}, a solution that is equally defensible from a statistical standpoint.

The numerical solution is iterated on the CDC 6600 computer (generally 3 times) until the maximum increment to the triangulated coordinates becomes < mm. Multiplying the normal equation matrix pertaining to the final iteration by its cor-

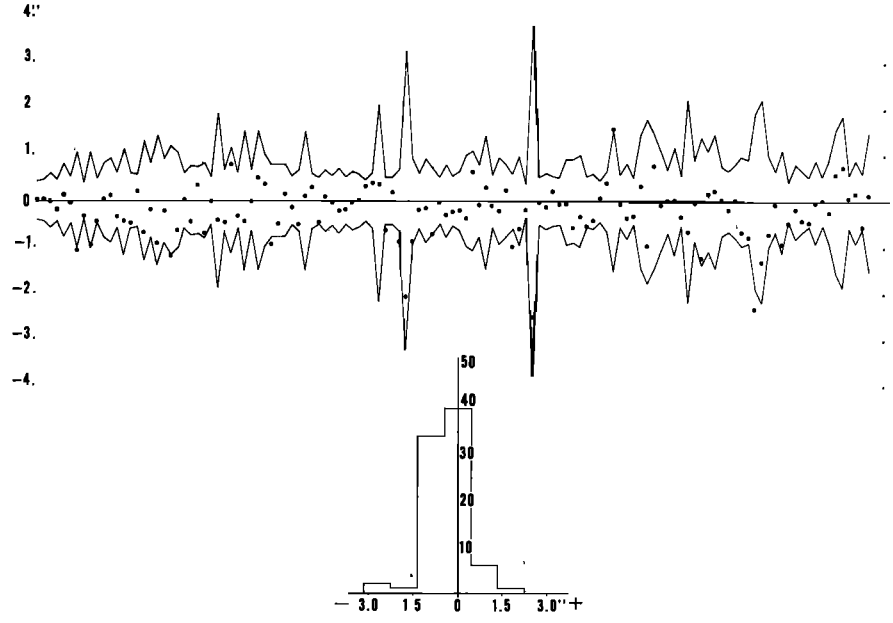

Fig. 17. Differences in azimuth, in seconds of arc, between directions computed as single-line adjustments and the corresponding figure from the final adjustment together with the 3σ value of the combined solution. The bottom figure is a histogram of these plotted values.

responding inverse matrix, one obtains as a check the expected unit matrix to within a unit in the tenth decimal place.

The mean error of unit weight after adjustment for all these solutions is 1.830 ± 0.014 against the expectation of 1.0, indicating the presence of additional unmodeled error sources. If the increase in the overall error budget can be ascribed to additional random error sources, then the effect is relatively harmless, the result being only a corresponding increase in the mean errors of the triangulated station positions. But if the effect of systematic errors, which are distributed in the adjustment in accordance with the least squares principle, is involved, the situation is more serious.

To gain some insight into the stability of the camera during the average half-hour period of operation, star photography taken immediately before and after the satellite transit was adjusted, and sets of camera orientation parameters were computed. Thus for each plate the change in azimuth ΔA and in elevation ΔE of the central ray with a corresponding rotation component $\Delta\chi$ was computed. The $\Delta\chi$ are random and completely within the range of their mean errors. The $\Delta A \cos E$ and especially the ΔE component, however, indicate the influence of a systematic error, as shown in Figures 15 and 16. For an evaluation of the diagrams it should be added that the individual Δ values shown have an average mean error of $\pm 0.5''$. Since star imagery is also available for the satellite transit period, it is possible to study these systematic changes

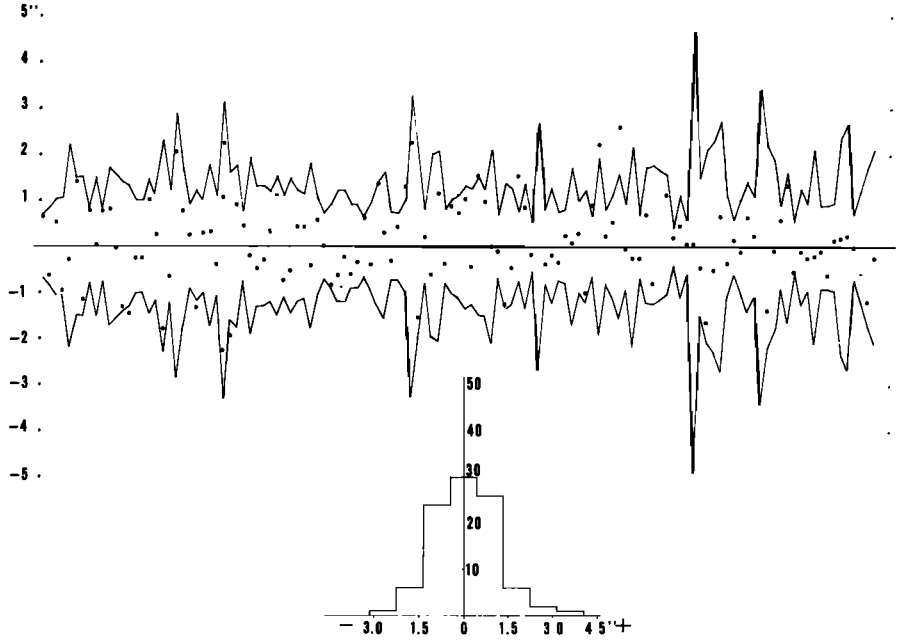

Fig. 18. The elevation differences of the data in Figure 17.

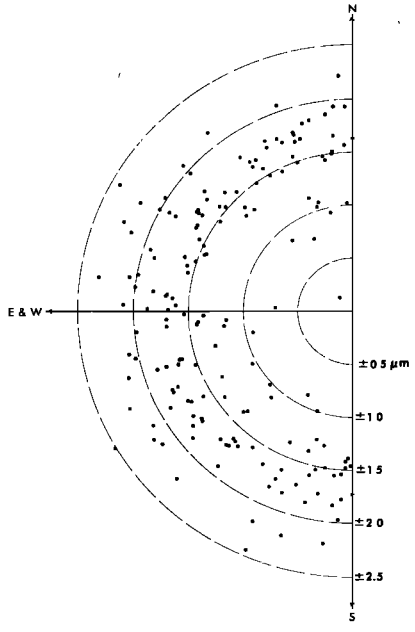

Fig. 19. Mean errors of unit weight σ after single-line adjustments plotted in azimuth of the line.

in orientation over the period of observation. A roughly linear trend with time is indicated.

To eliminate this source of error, orientation parameters that were based solely on star images obtained during the period of actual satellite transit were used in the final adjustment wherever possible. Still we cannot entirely escape the conclusion that the instability of the camera creates an additional error that, as the diagrams show, has a systematic component and acts as a source of additional accidental errors.

For a further analysis of the results it is important to realize that in consequence of the interpolation of each event into the astronomic system, absolute directions are obtained. This means that it is possible to triangulate the direction of the chord joining two adjacent stations in the net independently, i.e., with only the satellite passes observed from these two stations. Such computations were made for all 170 lines of the world net. In these adjustments, as well as in the final solution, all covariance matrices resulting from the individual processing steps were included, so that all results can be considered rigorously derived values. The line triangulations yield an average mean value for the ratio of mean error of unit weight before and after adjustment of 1:1.746, with a range of from 1:0.706 to 1:2.429. The theoretical expected average value is of course 1 : 1. This means that the observational data do not completely fill the accuracy expectations computed in the above cited partial analysis, a fact that was already mentioned in connection with the obtained mean error of unit weight after adjustment in the final triangulation. However, it is gratifying to note that this value increases only slightly from 1.746 for the average of all individual line adjustments to 1.830 for an adjustment based on the combination of all observations. These figures indicate that the entire body of data is apparently free of perturbing systematic errors and satisfies with practically no constraint the three-dimensional geometrical closure condition of the world net.

In order to strengthen this conclusion a comparison was made between the directions derived from the individual line adjustments and those of the combined solution. The resulting

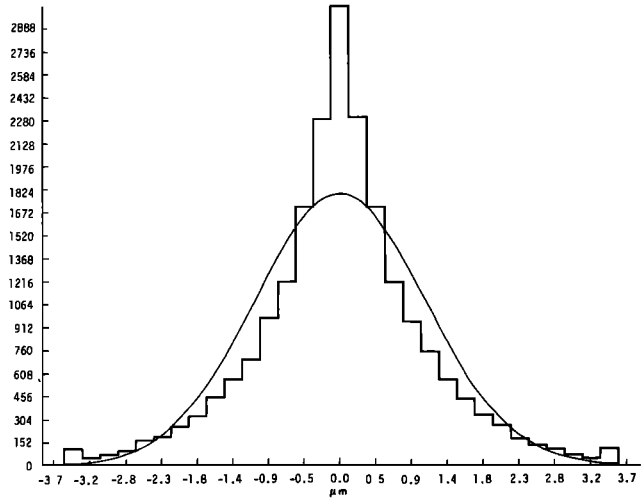

Fig. 20. Plate coordinate residuals for two-plate events (combined x and y values).

azimuth and elevation angle differences are shown in Figures 17 and 18 with their 3σ errors and are combined in histograms. Although these results do not fully meet ideal statistical expectations, it is not otherwise really possible to draw any conclusions regarding the presence of possible systematic error influences in the triangulations of the individual lines.

In order to analyze the accuracy of the shutter synchronization the following argument can be applied to the results of the individual line adjustments. Simple geometric considerations suggest that the larger the residual errors, due to synchronization discrepancies, in the spatial triangulation, the larger the angle is between the orbital plane of the satellite and the line to be triangulated. Because the Pageos satellite has an approximately polar orbit, it is sufficient to plot the mean error of unit weight after adjustment for the individual line adjustments versus the azimuth, or azimuth minus 180°, of the triangulated line. As Figure 19 shows, the distribution of these values is circular, and no dependence on azimuth can be detected. This test at least does not indicate the influence of any synchronization errors.

An examination of the statistical distribution of the 29104 residuals in the overall adjustment presents a further and ob-

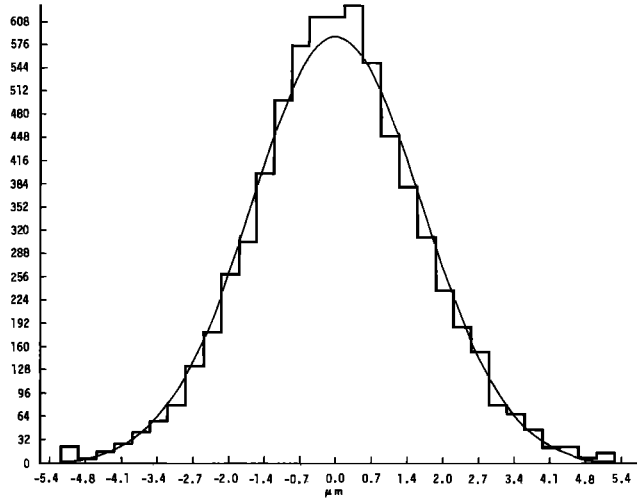

Fig. 21. Plate coordinate residuals for three-plate events (combined x and y values).

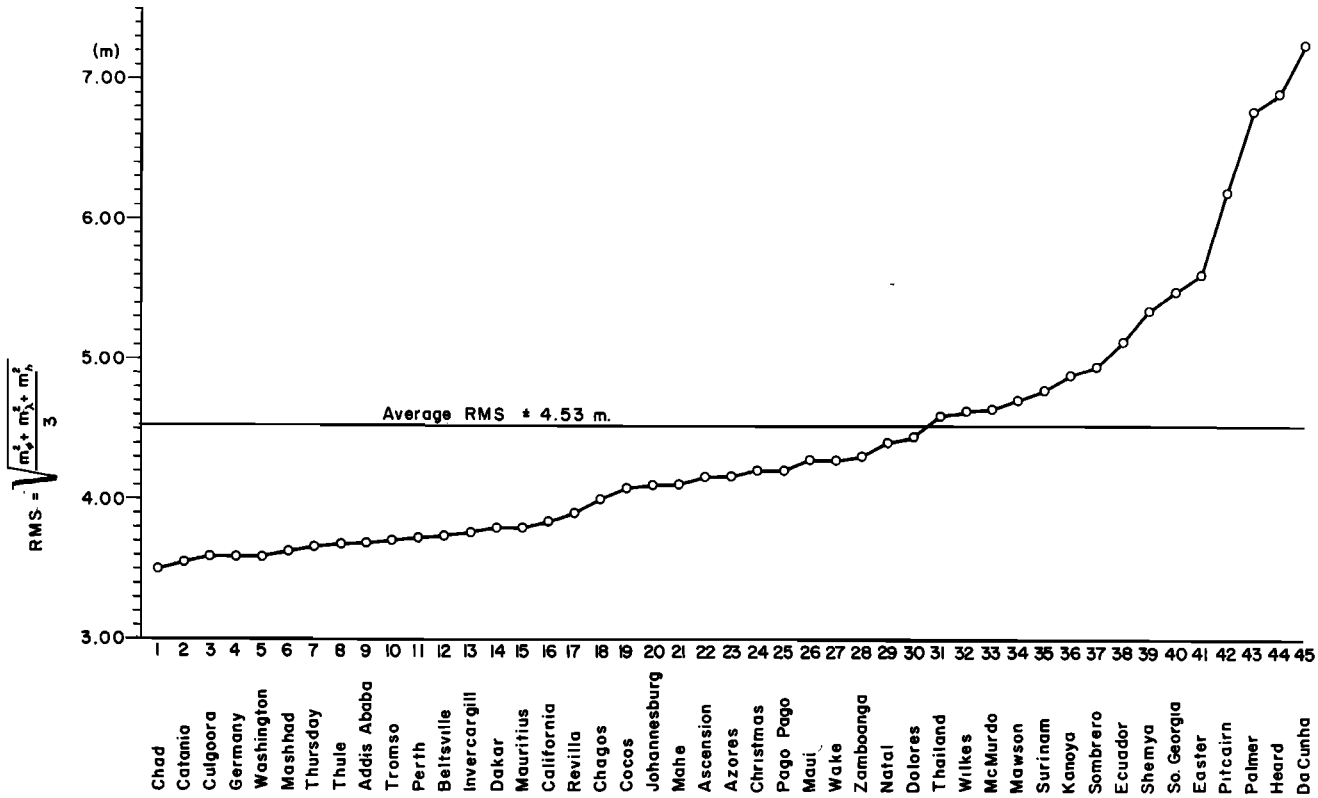

Fig. 22. The rms of mean coordinate errors of adjusted station positions.

TABLE 8. Coordinate Differences Between Transformed Doppler Solution and Translated BC-4 Solution After *XYZ* Fit

Station No. and Name	$\Delta\phi$, m	$\Delta\lambda$, m	Δh, m	Resultant
1, Thule	10.198	-2.216	10.464	14.779
2, Beltsville	-1.254	1.201	-4.516	4.839
3, Moses Lake	-3.072	5.628	-3.670	7.388
4, Shemya	5.711	13.780	15.061	21.198
6, Tromso	-1.451	-17.014	7.566	18.677
7, Azores	-10.097	-5.716	4.377	12.401
8, Surinam	0.002	1.959	-8.694	8.912
9, Quito	6.507	10.573	-7.272	14.388
11, Maui	4.162	-2.037	8.789	9.935
12, Wake	-14.550	-10.924	-24.453	30.479
13, Kanoya	6.458	0.116	3.956	7.574
15, Mashhad	3.600	4.048	1.256	5.561
16, Catania	1.740	-1.638	3.341	4.107
19, Dolores	-18.425	15.163	-4.296	24.245
20, Easter	7.924	13.930	3.152	16.333
22, Pago Pago	4.227	-6.107	-5.317	9.134
23, Thursday	-1.735	-7.291	-15.435	17.159
31, Invercargill	-7.362	-9.689	-5.584	13.389
32, Perth	3.261	0.162	0.665	3.332
38, Revilla	-5.298	0.445	3.129	6.169
40, Cocos	3.360	0.864	2.135	4.073
42, Addis Ababa	14.086	-1.952	5.724	15.329
43, Sombrero	-20.140	3.173	24.247	31.680
45, Mauritius	3.838	5.642	1.044	6.903
47, Zamboanga	3.162	3.466	-9.571	10.659
50, Palmer	-19.872	-5.176	12.703	24.147
53, McMurdo	-18.103	-1.576	-4.321	18.678
55, Ascension	-7.126	-10.677	0.245	12.838
59, Christmas	4.404	-4.747	-4.207	7.722
60, Culgoora	-12.420	-9.048	-2.916	15.641
63, Dakar	0.998	5.593	0.304	5.690
64, Chad	5.889	2.226	5.226	8.182
65, Hohenpeissenberg	5.497	-8.304	6.434	11.856
67, Natal	-10.375	-5.277	3.692	12.212
68, Johannesburg	1.352	2.525	-8.008	8.504
72, Thailand	3.350	6.659	-8.712	11.466
75, Mahé	8.413	0.122	-6.102	10.394

Δ equals BC-4 minus Doppler; rms values are ±8.916 m for $\Delta\phi$, ±7.179 m for $\Delta\lambda$, ±8.697 m for Δh, and ±14.376 m for resultant.

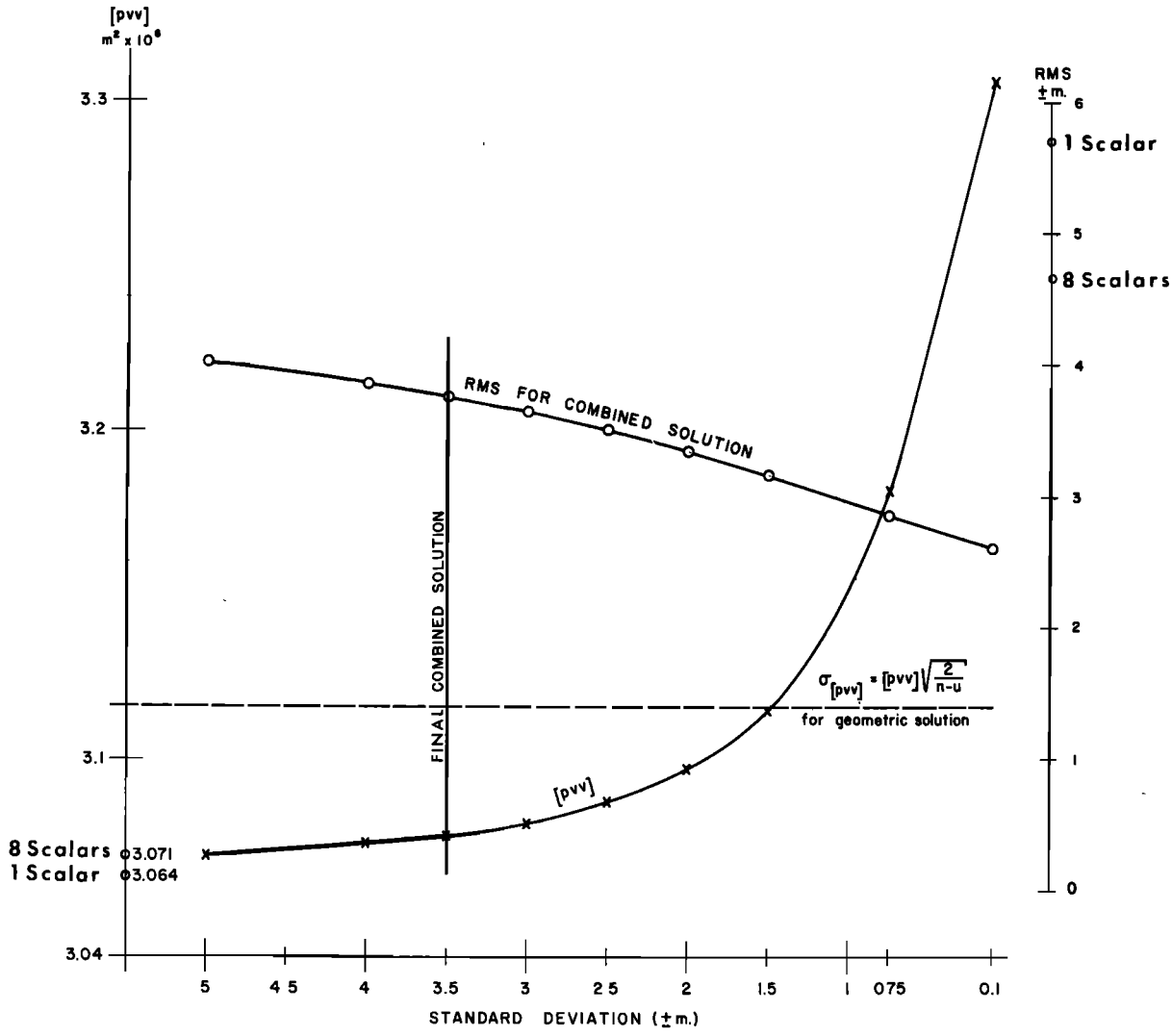

Fig. 23. Statistical results from nine combined solutions with varying weight assumptions for the colocated Doppler stations.

viously necessary opportunity to analyze the data. Figures 20 and 21 are histograms of the residuals in events that were observed from two and three stations, respectively. In order to compare these distributions with their theoretical normal distribution curves the residuals would have to be normalized, this process requiring the computation of the covariance matrix

$$\Sigma_v = \Sigma_\epsilon - AN^{-1}A^T\sigma_0^2 \tag{5}$$

This is, in the present case, a 29104 × 29104 completely filled square matrix, an obvious impossibility. As a result we are forced to neglect the geometric content of the second term of the expression and to normalize the residuals v approximately by dividing each with the mean error of the corresponding observation before adjustment. The greater the number of observations available for the determination of the position of the satellites or, in other words, the greater the number of stations observing the satellite, the more acceptable is the proposed approximation for the normalization of the residuals. This relationship may explain at least in part the fact that the fit of the normal curve to the histogram is better for the three-station events.

If one accepts the mean error of unit weight after adjustment as a significant measure for the inherent observational accuracy, we have mean coordinate errors for the triangulated stations as shown in Figure 22. It should be noted that although qualitatively the material at all stations is uniform, the quantity varies somewhat, the result being the variations of the coordinate errors.

Combination Solution

Based on the principles of celestial mechanics, the interpretation of the orbital parameters of satellites as derived from time-correlated observations permits not only the determination of the parameters of a mathematical model of the earth's gravitational field but in addition the three-dimensional positions of the satellite observing stations within a framework of coordinates referenced to the earth's mass center.

Satellite triangulation, on the other hand, is a measuring method in which the three-dimensional positions of a number of points of the earth's surface are established by purely geometric means.

Quite generally, satellite triangulation produces coordinates for the camera stations that should, in principle, agree except for a translation with the corresponding results from dynamic satellite geodesy, even though the methods are completely different in conceptual approach. This difference extends as well to the determination of scale, which in geometric satellite

TABLE 9. Three-Dimensional Cartesian Coordinates From Combined Final Solution

Station No. and Name	X, m	σ_X, m	Y, m	σ_Y, m	Z, m	σ_Z, m
1, Thule	546588.043	±2.524	1389976.770	±2.442	6180221.157	±3.191
2, Beltsville	1130783.206	±2.464	4830812.170	±2.853	3994691.260	±2.979
3, Moses Lake	-2127810.402	±2.337	3785844.188	±2.610	4656021.673	±2.896
4, Shemya	-3851759.714	±3.610	-396416.742	±3.622	5051324.861	±4.235
6, Tromso	2102943.362	±2.365	-721679.260	±2.697	5958170.871	±3.090
7, Azores	4433652.575	±3.091	2268128.968	±2.686	3971641.629	±3.327
8, Surinam	3623251.037	±3.166	5214216.431	±3.288	601536.293	±3.489
9, Quito	1280842.366	±3.158	6250939.190	±3.947	-10807.932	±3.487
11, Maui	-5466002.263	±3.288	2404414.762	±2.767	2242214.785	±3.235
12, Wake	-5858531.333	±3.287	-1394513.654	±2.966	2093798.651	±3.211
13, Kanoya	-3565848.055	±3.138	-4120713.101	±3.636	3303409.134	±3.581
15, Mashhad	2604363.535	±2.345	-4444158.701	±2.711	3750306.588	±2.712
16, Catania	4896401.374	±2.357	-1316181.910	±2.316	3856657.080	±2.572
19, Dolores	2280628.090	±2.674	4914528.492	±2.950	-3355416.607	±3.163
20, Easter	-1888587.555	±3.790	5354875.392	±3.952	-2895751.980	±3.784
22, Pago Pago	-6099939.342	±3.122	997345.983	±2.730	-1568582.700	±3.208
23, Thursday Isl.	-4955355.561	±2.613	-3842245.988	±2.427	-1163843.516	±2.534
31, Invercargill	-4313799.508	±2.680	-891345.724	±2.588	-4597253.294	±2.833
32, Perth	-2375382.732	±2.505	-4875545.638	±2.621	-3345387.849	±2.728
38, Revilla	-2160960.225	±2.510	5642694.520	±3.078	2035358.416	±3.176
39, Pitcairn	-3724745.647	±6.280	4421218.035	±5.694	-2686087.346	±5.255
40, Cocos	-741953.040	±3.161	-6190790.099	±3.069	-1338547.676	±2.752
42, Addis Ababa	4900753.422	±2.762	-3968244.643	±2.626	966329.417	±2.552
43, Sombrero	1371383.334	±2.724	3614745.095	±3.157	-5055927.530	±3.641
44, Heard	1098912.818	±5.747	-3684612.693	±6.212	-5071853.727	±7.780
45, Mauritius	3223440.444	±2.656	-5045332.006	±2.739	-2191798.454	±2.698
47, Zamboanga	-3361931.463	±2.812	-5365800.248	±3.094	763627.375	±3.330
50, Palmer	1192684.033	±3.433	2450986.983	±4.323	-5747037.701	±4.672
51, Mawson	1111352.024	±4.285	-2169264.675	±3.238	-5874322.862	±4.844
52, Wilkes	-902583.987	±3.525	-2409530.660	±3.232	-5816542.503	±4.730
53, McMurdo	-1310828.143	±3.356	-311271.145	±3.073	-6213265.956	±3.958
55, Ascension	6118342.544	±3.108	1571732.245	±2.883	-878608.379	±3.089
59, Christmas	-5885315.086	±3.027	2448357.151	±2.732	221669.643	±3.145
60, Culgoora	-4751621.039	±2.483	-2792063.383	±2.372	-3200156.628	±2.442
61, S. Georgia	2999924.593	±3.745	2219357.041	±4.232	-5155247.563	±4.886
63, Dakar	5884475.772	±2.853	1853478.486	±2.307	1612848.261	±2.930
64, Chad	6023393.960	±2.749	-1617940.871	±2.236	1331726.674	±2.508
65, Hohenpeissenberg	4213570.222	±2.356	-820837.313	±2.346	4702769.262	±2.758
67, Natal	5186415.778	±3.301	3653921.575	±3.208	-654288.938	±3.072
68, Johannesburg	5084832.837	±3.146	-2670338.698	±2.580	-2768083.655	±3.248
69, Da Cunha	4978430.027	±7.231	1086856.181	±5.644	-3823164.893	±7.581
72, Thailand	-941678.219	±3.661	-5967438.461	±3.337	2039300.514	±2.969
73, Chagos	1905147.827	±2.911	-6032272.479	±3.482	-810729.775	±3.001
75, Mahé	3602828.788	±3.024	-5238237.170	±3.096	-515947.433	±2.773
111, Wrightwood	-2448831.364	±2.679	4667972.160	±3.052	3582744.578	±3.162

triangulation is established by measuring the length of at least one side in the net by space traverse, whereas in dynamic satellite geodesy the scale is determined from the physical quantity GM (gravitational constant times mass of the earth).

The fundamental differences of the two methods provide the logical justification for the establishment of a worldwide geodetic system using both approaches, the method of dynamic satellite geodesy as well as that of geometric satellite triangulation. The basic equivalence of the results with respect to spatial coordination of the observation stations suggests a comparison and combination of such solutions.

R. J. Anderle of the Naval Weapons Laboratory, Dahlgren, Virginia, has kindly furnished the National Geodetic Survey a list of three-dimensional coordinates of 37 stations resulting from a dynamic solution and referenced to the mass center of the earth as origin. These stations are located in the close vicinity of BC-4 stations with the exception of five that are somewhat farther away. In each case the relative positions of the two neighboring stations were determined by a local survey tie. In order to make a valid comparison of the two solutions it is first necessary to translate the BC-4 coordinate system, which has an arbitrary origin, into the origin of the dynamic solution, the mass center, and to rotate the Doppler result about its z axis in order to make the two systems compatible with respect to longitude. However, in the comparison adjustment, two further rotations and a scale factor were modeled. These additional rotations give an indication of to what extent the orientations of the conventional pole-referenced rotation axes differ in the dynamic and the geometric solutions. Likewise, the scale factor reveals the difference in scale that, as was pointed out before, is derived in the one case from the product GM and in the other from the measured terrestrial base lines. The seven transformation parameters (three translations, three rotations, and a scale factor) were computed subject to a minimum condition on the sum of squares of residual coordinate differences, in the following referred to as XYZ fit.

The resulting mean discrepancy vector is 14.4 m, a value that is influenced by discrepancies larger than 20 m in five stations, as can be seen from the tabulation of the discrepancy vectors in Table 8. Anderle gives for the precision of his positions the standard deviations $\sigma_\phi = \pm 1.5$ m, $\sigma_\lambda = \pm 1.2$ m, and $\sigma_h = \pm 1.6$ m resulting in a station rms of ± 1.44 m. Considering the average standard deviation of the BC-4 system for these stations and neglecting for this cursory consideration the influence of the standard errors of the transformation parameters, we arrive at an expectation for a mean discrepancy vector of ± 4.35 m.

The difference between the actually obtained mean discrepancy vector of ±14.4 m and the statistically expected value of ±4.35 m shows that the two systems are not quite compatible within the range of their standard deviations. We cite now the transformation parameters obtained in this adjustment. Translation of BC-4 result into mass center (BC-4 plus Δ equals mass-centered BC-4 result) is

$$\Delta X = +19.590 \pm 1.342$$

$$\Delta Y = -17.684 \pm 1.325$$

$$\Delta Z = -14.344 \pm 1.506$$

Rotations of Doppler data to conform to translated BC-4 results are +0.6135″ ± 0.0451″ for X to Y (left-handed system), +0.1478″ ± 0.0572″ for Z to Y, and +0.0638″ ± 0.0563″ for Z to X. The scale factor to be applied to original Doppler data to conform to BC-4 system scale is

$$S = 0.9999977230 \pm 0.0000002476$$

An adjustment with three scale factors was also executed, resulting in

$$S_x = 0.9999973893 \pm 0.0000003560$$

$$S_y = 0.9999970923 \pm 0.0000003692$$

$$S_z = 0.9999989720 \pm 0.0000004397$$

The translation and rotation parameters were essentially the same as those obtained before.

As can be seen, the scale parameters in x and y agree with each other within the range of their standard deviations. The z scalar shows a significant deviation, which, however, reduces the average discrepancy vector after the XYZ fit by only 0.9 m. Therefore the following results were based on the solution that features only one scale factor. For this solution, Table 8 gives the remaining coordinate differences between the BC-4 system (Table 4) plus above given translation parameters and the rotated and scaled Doppler system. With the coordinate differences given in Table 8 and the translations and rotations

TABLE 10. Coordinate Differences Between Translated BC-4 Solution and Combined Solution After XYZ Fit

Station No. and Name	$\Delta\phi$, m	$\Delta\lambda$, m	Δh, m	Resultant, m
1, Thule	4.905	-0.684	3.289	5.945
2, Beltsville	0.185	2.209	-1.853	2.889
3, Moses Lake	-1.735	4.091	0.269	4.452
4, Shemya	1.505	4.864	9.935	11.164
6, Tromso	-1.757	-5.547	4.648	7.447
7, Azores	-0.822	-4.204	1.007	4.400
8, Surinam	0.515	2.110	-3.960	4.517
9, Quito	0.156	7.501	-2.580	7.933
11, Maui	0.582	-2.418	1.395	2.852
12, Wake	-2.316	-4.665	-8.936	10.343
13, Kanoya	5.430	-0.159	0.670	5.474
15, Mashhad	0.712	1.603	2.850	3.347
16, Catania	0.101	-3.388	3.223	4.677
19, Dolores	-10.566	4.851	3.581	12.165
20, Easter	-0.379	10.325	4.284	11.185
22, Pago Pago	0.561	-3.868	-2.642	4.718
23, Thursday Isl.	-0.403	-3.230	-5.313	6.231
31, Invercargill	-2.236	-5.096	-1.787	5.845
32, Perth	-2.256	1.600	-3.654	4.583
38, Revilla	-1.674	4.430	0.880	4.816
39, Pitcairn	0.968	1.486	1.936	2.625
40, Cocos	1.943	2.522	-1.498	3.518
42, Addis Ababa	3.113	0.599	1.303	3.427
43, Sombrero	-13.364	5.306	10.147	17.598
44, Heard	-1.623	3.003	-1.282	3.646
45, Mauritius	2.317	1.935	-1.021	3.187
47, Zamboanga	2.878	0.990	-4.290	5.260
50, Palmer	-17.711	1.139	12.169	21.519
51, Mawson	-1.968	3.462	-0.566	4.022
52, Wilkes	-5.689	1.977	-1.901	6.315
53, McMurdo	-5.707	-3.880	-0.698	6.936
55, Ascension	-2.133	-4.243	1.390	4.948
59, Christmas	-0.003	-2.663	-1.335	2.978
60, Culgoora	-2.556	-4.203	-3.594	6.092
61, S. Georgia	-13.290	-3.515	8.088	15.950
63, Dakar	-0.078	-3.618	0.264	3.628
64, Chad	0.396	-1.160	1.656	2.060
65, Hohenpeissenberg	0.397	-4.163	4.660	6.261
67, Natal	-3.810	-3.519	0.459	5.207
68, Johannesburg	1.930	0.627	-2.082	2.908
69, Da Cunha	-7.851	-6.563	6.722	12.243
72, Thailand	3.621	4.358	-2.717	6.284
73, Chagos	3.124	1.925	-1.213	3.865
75, Mahé	3.651	1.386	-1.143	4.069
78, Vila Efate	0.192	-4.949	-3.148	5.868
111, Wrightwood	-0.250	4.706	0.827	4.784
123, Point Barrow	-0.378	6.691	4.322	7.974

Δ equals BC-4 solution minus combined solution. The rms values are ±4.817 m for $\Delta\phi$, ±3.974 m for $\Delta\lambda$, ±4.183 m for Δh, and ±7.516 m for resultant; n = 47.

TABLE 11. Coordinate Differences Between Transformed Doppler Solution and Combined Solution After *XYZ* Fit

Station No. and Name	$\Delta\phi$, m	$\Delta\lambda$, m	Δh, m	Resultant, m
1, Thule	4.948	-1.690	7.309	8.987
2, Beltsville	-2.044	-0.855	-2.602	3.418
3, Moses Lake	-1.540	1.573	-3.619	4.236
4, Shemya	4.433	8.980	5.727	11.537
6, Tromso	-0.062	-11.187	3.029	11.590
7, Azores	-10.072	-1.351	3.282	10.679
8, Surinam	-1.574	0.269	-4.707	4.970
9, Quito	5.469	3.704	-4.496	7.991
11, Maui	3.717	0.755	8.146	8.986
12, Wake	-11.845	-6.005	-14.576	19.718
13, Kanoya	1.320	0.417	4.100	4.327
15, Mashhad	2.605	2.585	-1.262	3.881
16, Catania	0.976	1.908	0.143	2.148
19, Dolores	-9.064	11.106	-7.536	16.195
20, Easter	7.860	4.731	-0.514	9.188
22, Pago Pago	4.182	-1.580	-1.630	4.758
23, Thursday Isl.	-0.665	-3.988	-8.993	9.860
31, Invercargill	-4.103	-4.126	-2.665	6.400
32, Perth	6.200	-1.870	5.400	8.432
38, Revilla	-4.009	-3.528	2.629	5.953
40, Cocos	1.678	-2.067	4.543	5.265
42, Addis Ababa	10.339	-2.729	4.697	11.679
43, Sombrero	-7.959	-1.174	14.647	16.711
45, Mauritius	1.132	3.045	2.671	4.206
47, Zamboanga	0.682	2.454	-4.308	5.004
50, Palmer	-3.410	-5.423	1.174	6.512
53, McMurdo	-11.079	2.695	-2.663	11.709
55, Ascension	-6.249	-6.384	-1.088	9.000
59, Christmas	4.643	-1.483	-1.990	5.265
60, Culgoora	-8.968	-4.719	1.850	10.302
63, Dakar	0.028	9.353	-0.024	9.354
64, Chad	4.612	3.340	3.648	6.763
65, Hohenpeissenberg	4.508	-3.934	1.788	6.244
67, Natal	-7.821	-1.469	3.266	8.602
68, Johannesburg	-1.506	1.312	-5.527	5.876
72, Thailand	-0.145	2.282	-5.246	5.723
75, Mahé	4.334	-1.677	-4.459	6.441

Δ equals combined solution minus Doppler; rms values are $\pm$5.588 m for $\Delta\phi$, $\pm$4.436 m for $\Delta\lambda$, $\pm$5.339 m for Δh, and $\pm$8.911 m for resultant.

given before, it is a straightforward matter to compute backwards from the BC-4 result (Table 4) to the original given Doppler station data. The translated BC-4 system itself represents the strictly geometric result referenced to the mass center of the dynamic solutions.

The problem for a combined solution is now to average the coordinate values as obtained for the translated BC-4 system and the rotated and scaled Doppler system. In recognition that the two transformed systems differ, as is expressed by a rms discrepancy vector of 14.4 m, more than 3 times the amount expected from the individual solution accuracy statements, a combination solution becomes a question of the weight ratio between the two solutions. To shed light on this question, the geometric satellite triangulation system was adjusted several times, the transformed Doppler position coordinates for the given 37 stations with various weights being introduced as constraints. The critical evaluation of these adjustments was made in relation to the individually obtained sum of squares of the weighted residuals for the geometric solution, a quantity that because of its straightforward meaning is believed to be quite a reliable indicator. The following graph (Figure 23) shows the sum of the *pvv* versus the various weight assumptions made for the Doppler results covering a range from $\pm$0.1 m to $\pm$5.0 m for each of the given Doppler derived coordinates. On the left side the *pvv* sum is given as it is obtained from the strictly geometric solution (without any Doppler station constraint) for the one and eight scalar solutions mentioned earlier. The dotted line indicates the standard deviation associated with the *pvv* sum.

From the [*pvv*] curve one can see, as was to be expected, that an essentially rigorous enforcement of the Doppler result (standard deviation of $\pm$0.1 m) increases the [*pvv*] drastically; in other words, the integrity of the geometric triangulation is impaired. On the other hand, a weighting in accordance with a standard deviation of $\pm$5 m results in a *pvv* sum identical to the one obtained from a strictly geometric adjustment by using the eight scale lines as constraints.

It is now unquestionably a decision of personal preference as to which weighting factor for the dynamic solution to accept as defensible for a combination result, at least in the range from $\pm$2.5 to $\pm$4.0 m. On the other hand, the resulting differences in the mean station coordinate discrepancy vectors between these two solutions are rather small, amounting in latitude to 1.5 m, in longitude to 1.2 m, and in height to 1.6 m. In order to keep the increase in the [*pvv*] small, when it is compared with the strictly geometric solution, a weighting in accordance with a standard deviation of $\pm$3.5 m for all Doppler coordinates was adopted. The solution was further constrained by the scalars, all weighted in accordance with a standard deviation of 1 part in 2 million. Table 9 gives the result of this adjustment and the associated standard deviations for the triangulated coordinates. Tables 10 and 11 show coordinate differences between the combined solution and the BC-4 and Doppler solutions, respectively. The mean error of unit weight

after adjustment is 1.830 ± 0.13, the same as that for the purely geometric solution.

A comparison between the two sets of 29104 residual errors from the purely geometric adjustment and the adjustment enforcing the Doppler results was made. These Δv values have a mean of +0.001 μm. The maximum values encountered are −0.537 μm and +0.451 μm.

As a by-product the standard deviation for each event is computed in each triangulation adjustment. A comparison of these standard deviations between the purely geometric and the combined solution shows that the range for these values in the geometric solution is from ±0.281 μm to ±3.462 μm and for the combined solution from ±0.251 μm to ±3.468 μm.

This statistical information is presented to give evidence that in the combined solution, no undue strain on the observational data of the geometric satellite triangulation is present.

Derived Geodetic Parameters

The semimajor axis a and the flattening f of a reference ellipsoid may be regarded as the basic parameters for a geodetic world system, its center coinciding with the earth's center of mass. The direction of the Z axis, i.e. the earth's rotation axis, is fixed by the conventionally adopted mean pole position at a specified epoch and the direction of the X axis through the null meridian by an identifiable point on the surface of the earth.

With the establishment of such a reference system the XYZ coordinates of the combined solution as given in Table 9 can be transformed into latitude, longitude, and ellipsoid height. Furthermore, classical geodetic results referenced to individual datum ellipsoids can be transformed to such a world system.

Using the values presented for the determination of these quantities, we arrive at the following results. To begin with, the station coordinates obtained in the geometric satellite triangulation solution (Table 4), reduced to sea level, were adjusted to a best-fitting ellipsoid of revolution. The significance of such a solution is somewhat dubious in view of the fact that only 43 stations are available for which leveling heights were obtained and that there is no a priori evidence that the mean of the corresponding geoid heights is close to zero. The result is shown in the first row of Table 12. The resulting translations ΔX, ΔY, ΔZ on line 1 as well as those shown on lines 2, 6, 7, and 11 for other solutions are not significant in themselves because they depend entirely on the approximation values for the mass-centered coordinates, introduced for the origin of the geometric solution. Only their consistency in the various solutions is of interest.

The second solution is a repetition of the first with the flattening f = 1/298.250, held fixed, a value that is derived by dynamic satellite geodesy methods and is presently considered to be reliable. This result is on line 2. Furthermore, ellipsoid fits were executed, the results of the combined solution resembling otherwise the solutions presented on lines 1 and 2. These results are given on lines 3 and 4, respectively. Here, as on lines 8 and 9, the ΔX, ΔY, ΔZ indicate to what extent the coordinate origin of the specific solution differs from the mass center of the dynamic solution. Still another computation was performed, the combined solution holding the original position of Anderle's mass center fixed. In this solution, only the semimajor axis a was determined. This result is shown on line 5. With the same raw material these ellipsoid fit solutions were repeated, the geoid heights as computed from raw data published by *Anderle* [1973] being incorporated. The corresponding results are shown on lines 6–10. On line 11 the result of the station-to-station least squares fit, based on the

TABLE 12. Best-Fitting Ellipsoid Parameters

	Input	Additional Data	Type of Solution	a, 6,378,••• m	$1/f$	ΔX, m	ΔY, m	ΔZ, m
1.	BC-4 result, 43 stations	msl elevations	unconstrained ellipsoid fit	130.17	298.377	+16.20	-14.82	-16.40
2.	BC-4 result, 43 stations	msl elevations	ellipsoid fit constrained to dynamically determined $1/f$	132.80	298.250	+16.29	-15.32	-16.74
3.	Combined solution, 43 stations	msl elevations	unconstrained ellipsoid fit	133.98	298.246	+1.373	+2.434	-1.844
4.	Combined solution, 43 stations	msl elevations	ellipsoid fit constrained to dynamically determined $1/f$	133.90	298.250	+1.370	+2.453	-1.835
5.	Combined solution, 43 stations	msl elevations	ellipsoid fit constrained to dynamically determined $1/f$ and to Anderle mass center position	134.02	298.250	0	0	0
6.	BC-4 result, 37 stations	msl elevations and Anderle geoidal heights N	unconstrained ellipsoid fit	126.47	298.409	+14.702	-19.482	-13.816
7.	BC-4 result, 37 stations	msl elevations and Anderle geoidal heights N	ellipsoid fit constrained to dynamically determined $1/f$	129.45	298.250	+15.140	-20.181	-15.252
8.	Combined solution, 37 stations	msl elevations and Anderle geoidal heights N	unconstrained ellipsoid fit	128.83	298.322	-1.9000	+0.378	+1.183
9.	Combined solution, 37 stations	msl elevations and Anderle geoidal heights N	ellipsoid fit constrained to dynamically determined $1/f$	130.21	298.250	-1.756	-0.764	+0.721
10.	Combined solution, 37 stations	msl elevations and Anderle geoidal heights N	ellipsoid fit constrained to dynamically determined $1/f$ and to Anderle mass center position	130.22	298.250	0	0	0
11.	BC-4 result Doppler result, 37 stations	none	*XYZ* fit between Doppler and BC-4 result	130.48 ±1.58	•••	+19.590 ±1.34	-17.684 ±1.33	-14.344 ±1.51

after adjustment is 1.830 ± 0.13, the same as that for the purely geometric solution.

A comparison between the two sets of 29104 residual errors from the purely geometric adjustment and the adjustment enforcing the Doppler results was made. These Δv values have a mean of +0.001 μm. The maximum values encountered are −0.537 μm and +0.451 μm.

As a by-product the standard deviation for each event is computed in each triangulation adjustment. A comparison of these standard deviations between the purely geometric and the combined solution shows that the range for these values in the geometric solution is from ±0.281 μm to ±3.462 μm and for the combined solution from ±0.251 μm to ±3.468 μm.

This statistical information is presented to give evidence that in the combined solution, no undue strain on the observational data of the geometric satellite triangulation is present.

Derived Geodetic Parameters

The semimajor axis a and the flattening f of a reference ellipsoid may be regarded as the basic parameters for a geodetic world system, its center coinciding with the earth's center of mass. The direction of the Z axis, i.e. the earth's rotation axis, is fixed by the conventionally adopted mean pole position at a specified epoch and the direction of the X axis through the null meridian by an identifiable point on the surface of the earth.

With the establishment of such a reference system the XYZ coordinates of the combined solution as given in Table 9 can be transformed into latitude, longitude, and ellipsoid height. Furthermore, classical geodetic results referenced to individual datum ellipsoids can be transformed to such a world system.

Using the values presented for the determination of these quantities, we arrive at the following results. To begin with, the station coordinates obtained in the geometric satellite triangulation solution (Table 4), reduced to sea level, were adjusted to a best-fitting ellipsoid of revolution. The significance of such a solution is somewhat dubious in view of the fact that only 43 stations are available for which leveling heights were obtained and that there is no a priori evidence that the mean of the corresponding geoid heights is close to zero. The result is shown in the first row of Table 12. The resulting translations ΔX, ΔY, ΔZ on line 1 as well as those shown on lines 2, 6, 7, and 11 for other solutions are not significant in themselves because they depend entirely on the approximation values for the mass-centered coordinates, introduced for the origin of the geometric solution. Only their consistency in the various solutions is of interest.

The second solution is a repetition of the first with the flattening f = 1/298.250, held fixed, a value that is derived by dynamic satellite geodesy methods and is presently considered to be reliable. This result is on line 2. Furthermore, ellipsoid fits were executed, the results of the combined solution resembling otherwise the solutions presented on lines 1 and 2. These results are given on lines 3 and 4, respectively. Here, as on lines 8 and 9, the ΔX, ΔY, ΔZ indicate to what extent the coordinate origin of the specific solution differs from the mass center of the dynamic solution. Still another computation was performed, the combined solution holding the original position of Anderle's mass center fixed. In this solution, only the semimajor axis a was determined. This result is shown on line 5. With the same raw material these ellipsoid fit solutions were repeated, the geoid heights as computed from raw data published by *Anderle* [1973] being incorporated. The corresponding results are shown on lines 6–10. On line 11 the result of the station-to-station least squares fit, based on the

TABLE 12. Best-Fitting Ellipsoid Parameters

	Input	Additional Data	Type of Solution	a, 6,378,••• m	$1/f$	ΔX, m	ΔY, m	ΔZ, m
1.	BC-4 result, 43 stations	msl elevations	unconstrained ellipsoid fit	130.17	298.377	+16.20	-14.82	-16.40
2.	BC-4 result, 43 stations	msl elevations	ellipsoid fit constrained to dynamically determined $1/f$	132.80	298.250	+16.29	-15.32	-16.74
3.	Combined solution, 43 stations	msl elevations	unconstrained ellipsoid fit	133.98	298.246	+1.373	+2.434	-1.844
4.	Combined solution, 43 stations	msl elevations	ellipsoid fit constrained to dynamically determined $1/f$	133.90	298.250	+1.370	+2.453	-1.835
5.	Combined solution, 43 stations	msl elevations	ellipsoid fit constrained to dynamically determined $1/f$ and to Anderle mass center position	134.02	298.250	0	0	0
6.	BC-4 result, 37 stations	msl elevations and Anderle geoidal heights N	unconstrained ellipsoid fit	126.47	298.409	+14.702	-19.482	-13.816
7.	BC-4 result, 37 stations	msl elevations and Anderle geoidal heights N	ellipsoid fit constrained to dynamically determined $1/f$	129.45	298.250	+15.140	-20.181	-15.252
8.	Combined solution, 37 stations	msl elevations and Anderle geoidal heights N	unconstrained ellipsoid fit	128.83	298.322	-1.9000	+0.378	+1.183
9.	Combined solution, 37 stations	msl elevations and Anderle geoidal heights N	ellipsoid fit constrained to dynamically determined $1/f$	130.21	298.250	-1.756	-0.764	+0.721
10.	Combined solution, 37 stations	msl elevations and Anderle geoidal heights N	ellipsoid fit constrained to dynamically determined $1/f$ and to Anderle mass center position	130.22	298.250	0	0	0
11.	BC-4 result Doppler result, 37 stations	none	XYZ fit between Doppler and BC-4 result	130.48 ±1.58	•••	+19.590 ±1.34	-17.684 ±1.33	-14.344 ±1.51

matching of the positions of 37 stations as determined by the geometric and the dynamic method, is shown.

From the information presented in Table 12 it was concluded that a reference ellipsoid with $1/f = 298.250$ and a semimajor axis of 6,378,130 m would correspond best to the available information.

Table 13 gives the corresponding latitude, longitude (east), and ellipsoid heights with their respective standard deviations computed from the XYZ coordinates of the combined solution (Table 9).

In Table 14 the survey data are given. A comparison of the result presented in Table 13 with the results of astronomical position observations and the values of mean sea level observations, as given with the survey data, allows the computation of plumb line deflections and the determination of geoid heights. The corresponding results are tabulated in Tables 15 and 16, respectively.

The $\Delta\lambda$ values in Table 15 refer in accordance with the given geographic coordinates on Table 13 to a system of east longitude, with the conventional designation astro minus geodetic equals Δ. The $\Delta\phi$ values represent absolute position deflections in the meridian of the station, positive to the south. The computed η values, positive to the east, however, depend quantitatively on the chosen position of the null meridian of the combined solution. In order to average them out an additional rotation in longitude would be necessary, which would have to be added as a constant to all longitudes tabulated in Table 13. Such a correction amounts to

$$\Delta\lambda = \frac{\sum_i^i (\lambda_A - \lambda_G)_i \cos\phi_i}{\sum_i^i \cos\phi_i} = -0.485'' \qquad (6)$$

(east longitudes positive). The significance of such a correction is, however, impaired by the relatively small number of plumb line deflections available.

Table 16 gives the geoid heights as computed from the combined solution (Table 13) and the msl elevations of the survey data. For comparison the geoid heights as obtained by Anderle from the dynamic solution are given in the second column, and the corresponding differences are given in the column labeled ΔN.

With the exception of stations 11 (Hawaii), 12 (Wake), 13 (Japan), and 43 (Sombrero) these Δ values are well within the expected level of accuracy. Obviously, both sets of N values are also affected by the uncertainties in mean sea level for the various datums, to which the leveling data are referred.

TABLE 13. Geographic Coordinates From Combined Solution Computed With a = 6378130 m and f = 1:298.250

Station No. and Name	Latitude	σ_ϕ, m	Longitude	σ_λ, m	Ellipsoid Height, m	σ_h, m
1, Thule	76°30'4.8627"N	2.184	291°27'59.4280"E	2.675	219.379	3.236
2, Beltsville	39°01'39.3318"N	2.540	283°10'27.9765"E	2.440	-1.458	3.264
3, Moses Lake	47°11'6.6534"N	2.424	240°39'43.5760"E	2.308	336.069	3.069
4, Shemya	52°42'48.9705"N	3.782	174°7'26.0462"E	3.475	39.745	4.193
6, Tromso	69°39'44.4978"N	2.361	18°56'27.5273"E	2.535	133.357	3.211
7, Azores	38°45'36.0847"N	2.864	332°54'25.2813"E	2.652	108.829	3.546
8, Surinam	05°26'53.4378"N	3.457	304°47'40.6928"E	2.880	-20.115	3.585
9, Quito	0°5'51.7281"S	3.504	281°34'47.4488"E	3.163	2694.047	3.937
11, Maui	20°42'26.9218"N	3.045	203°44'38.3808"E	2.696	3075.656	3.522
12, Wake	19°17'28.2961"N	2.947	166°36'39.4948"E	2.896	4.297	3.589
13, Kanoya	31°23'42.5648"N	3.278	130°52'16.2716"E	3.390	83.416	3.694
15, Mashhad	36°14'25.5340"N	2.441	59°37'43.9207"E	2.459	963.436	2.860
16, Catania	37°26'38.5025"N	2.158	15°2'44.8491"E	2.240	45.972	2.800
19, Dolores	31°56'35.5287"S	2.992	294°53'38.5873"E	2.579	627.599	3.203
20, Easter	27°10'36.4176"S	3.317	250°34'22.7515"E	3.544	219.755	4.554
22, Pago Pago	14°19'54.4748"S	3.141	189°17'8.7112"E	2.701	35.347	3.223
23, Thursday Isl.	10°35'2.9982"S	2.511	142°12'39.5544"E	2.341	119.259	2.718
31, Invercargill	46°24'58.1142"S	2.542	168°19'31.6698"E	2.588	-0.007	2.949
32, Perth	31°50'24.9112"S	2.482	115°58'31.8154"E	2.420	-8.327	2.927
38, Revilla	18°43'58.2071"N	3.020	249°2'41.4901"E	2.515	-14.701	3.235
39, Pitcairn	25°4'6.8403"S	3.686	229°53'12.6661"E	4.975	317.220	7.817
40, Cocos	12°11'44.0207"S	2.682	96°50'3.0512"E	3.132	-29.827	3.163
42, Addis Ababa	8°46'12.5193"N	2.574	38°59'52.1902"E	2.607	1872.647	2.766
43, Sombrero	52°46'52.5872"S	3.472	290°46'33.7413"E	2.662	95.214	3.378
44, Heard	53°1'9.0693"S	6.472	73°23'35.2173"E	6.032	39.662	7.314
45, Mauritius	20°13'53.1132"S	2.586	57°25'32.4106"E	2.634	137.814	2.869
47, Zamboanga	6°55'20.7741"N	3.324	122°4'8.8287"E	2.696	71.335	3.215
50, Palmer	64°46'26.7693"S	4.870	295°56'53.4936"E	3.289	26.028	4.184
51, Mawson	67°36'4.8017"S	3.925	62°52'23.3298"E	3.829	39.813	4.690
52, Wilkes	66°16'44.9811"S	3.267	110°32'7.4526"E	3.359	10.755	4.808
53, McMurdo	77°50'41.6571"S	3.445	166°38'30.7416"E	3.006	-41.095	3.907
55, Ascension	7°58'15.4065"S	3.058	345°35'34.4179"E	2.943	83.939	3.092
59, Christmas	2°0'18.3902"N	3.148	202°35'16.2920"E	2.593	24.514	3.157
60, Culgoora	30°18'34.2631"S	2.339	149°33'41.0676"E	2.275	235.088	2.666
61, S. Georgia	54°17'1.1326"S	3.750	323°30'20.9006"E	4.454	19.203	4.659
63, Dakar	14°44'42.1988"N	2.847	342°31'0.2512"E	2.306	55.378	2.945
64, Chad	12°7'54.5921"N	2.520	15°2'7.0547"E	2.223	306.766	2.756
65, Hohenpeissenberg	47°48'3.9953"N	2.184	11°1'25.0048"E	2.296	977.952	2.928
67, Natal	5°55'39.0642"S	3.061	324°50'4.6598"E	3.199	38.288	3.328
68, Johannesburg	25°52'59.1717"S	2.975	27°42'23.5867"E	2.587	1536.885	3.402
69, Da Cunha	37°3'53.6135"S	6.418	347°41'5.3077"E	5.714	45.432	8.227
72, Thailand	18°46'10.5737"N	2.770	98°58'2.9441"E	3.622	259.580	3.545
73, Chagos	7°21'6.6304"S	2.994	72°28'21.1236"E	2.969	-72.915	3.446
75, Mahé	4°40'14.6759"S	2.753	55°28'48.1258"E	2.830	545.382	3.298
111, Wrightwood	34°22'54.4315"N	2.628	242°19'6.1310"E	2.757	2252.261	3.457

TABLE 14. Survey Coordinates of BC-4 Stations

BC-4 Station No. and Name	Geodetic Coordinates		Astronomic Coordinates		Elevation of Reference Point Above msl, m	N, m	Datum	Ellipsoid
	ϕ_G	λ_G	ϕ_A	λ_A				
001, Thule	76°30'05.3226"N	68°32'33.1709"W	76°30'11.67"N	68°32'48.91"W	206.0	+32.0	Qornoq	International
002, Beltsville	39°01'39.003"N	76°49'33.058"W	39°01'37.73"N	76°49'24.65"W	44.3	-0.4	North American 1927	Clarke 1866
003, Moses Lake	47°11'07.1324"N	119°20'11.8815"W	47°11'03.24"N	119°20'17.05"W	368.74	-16.0	North American 1927	Clarke 1866
004, Shemya	52°42'54.8940"N	185°52'22.1299"W	52°43'03.48"N	185°52'15.08"W	36.76	-46.0	North American 1927	Clarke 1866
006, Tromso	69°39'44.2901"N	341°03'27.6743"W	69°39'43.24"N	341°03'12.96"W	106.0	+12.6	European	International
007, Azores	38°45'36.7250"N	27°05'38.9360"W	38°45'43.28"N	27°05'24.59"W	53.26	...	SW Base	International
008, Surinam	05°27'04.9824"N	55°12'13.9921"W	05°26'48.96"N	55°12'21.21"W	18.38	+3.0	Provisional South American 1956	International
009, Quito	00°05'50.4680"S	78°25'10.7875"W	00°05'53.09"S	78°25'03.09"W	2682.1	+24.6	South American 1969	South American
011, Maui	20°42'38.5610"N	156°15'31.4711"W	20°42'21.86"N	156°15'22.95"W	3049.27	...	Old Hawaiian	Clarke 1866
012, Wake	19°17'23.2275"N	193°23'20.2197"W	19°17'24.40"N	193°23'34.82"W	3.46	...	Astro 1952	International
013, Kanoya	31°23'30.13971"N	229°07'35.14051"W	31°23'38.48"N	229°07'34.29"W	65.90	+27.0	Tokyo	Bessel
015, Mashhad	36°14'29.5269"N	300°22'17.2712"W	36°14'27.82"N	300°21'59.20"W	991.05	-38.0	European 1950	International
016, Catania	37°26'42.3451"N	344°57'12.3041"W	37°26'38.70"N	344°56'56.81"W	9.00	-16.6	European	International
019, Villa Dolores	31°56'33.9540"S	65°06'18.658"W	...	...	608.18	+13.0	South American 1969	South American
020, Easter Isl.	27°10'39.2132"S	109°25'42.5051"W	27°10'39.21"S	109°25'42.51"W	230.8	...	Astro 1967	International
022, Pago Pago	14°20'12.216"S	170°42'46.758"W	14°20'08.34"S	170°42'52.15"W	5.34	+22.0	Samoa 1962	Clarke 1866
023, Thursday Isl.	10°35'08.0374"S	217°47'24.5045"W	10°35'06.78"S	217°47'25.11"W	59.6	-4.6	Australian National	Australian National
031, Invercargill	46°25'03.4908"S	191°40'28.8448"W	46°25'01.05"S	191°40'25.10"W	0.95	...	Geodetic 1949	International
032, Perth	31°50'28.9922"S	244°01'33.3824"W	31°50'24.57"S	244°01'56.28"W	26.30	+15.4	Australian National	Australian National
038, Revilla	18°43'44.93"N	110°57'20.72"W	18°43'44.93"N	110°57'20.72"W	23.20	...	Isla Socorro Astro	Clarke 1866
039, Pitcairn	25°04'07.1461"S	130°06'48.1184"W	25°04'07.15"S	130°06'48.12"W	339.39	...	Pitcairn Astro 1967	International
040, Cocos	...	...	12°11'57.91"S	263°10'12.92"W	4.41	...	Anna Astro 1965	Australian National
042, Addis Ababa	08°46'08.5013"N	321°00'10.8355"W	08°46'05.74"N	321°00'02.81"W	1886.46	-8.0	Adindan	Clarke 1880
043, Cerro Sombrero	52°46'52.4683"S	69°13'30.4273"W	52°46'50.74"S	69°13'33.56"W	80.66	...	Provisional South Chile 1963	International
044, Heard Isl.	...	...	53°01'12.0309"S	286°36'32.5846"W	3.771	...	Astro 1969	International
045, Mauritius	20°13'41.942"S	302°34'52.339"W	20°13'37.48"S	302°35'07.20"W	138.2	...	Le Ponce Astro	Clarke 1880
047, Zamboanga	06°55'26.132"N	237°55'55.162"W	06°55'18.29"N	237°55'53.55"W	9.391	...	Luzon	Clarke 1886
050, Palmer	...	...	64°46'33.98"S	64°03'22.96"W	16.44	...	Palmer Astro 1969	Clarke 1880
051, Mawson	...	...	67°36'03.08"S	297°07'35.59"W	11.3	...	Astro 1969	
052, Wilkes (Casey)	...	...	66°16'45.12"S	249°27'55.39"W	18.0	...	Astro 1969	
053, McMurdo	77°50'46.2487"S	193°21'52.4155"W	77°50'43.32"S	193°21'46.14"W	19.09	...	Camp Area Astro 1961-1962 USGS	International
055, Ascension	07°58'16.6342"S	14°24'27.2363"W	07°58'18.27"S	14°24'30.36"W	70.94	...	Ascension Isl. 1958	International
059, Christmas Isl.	...	...	02°00'35.622"N	157°24'38.038"W	2.75	...	Christmas Isl. 1967 Astro	International
060, Culgoora	30°18'39.4182"S	210°26'23.1079"W	30°18'36.14"S	210°26'28.89"W	211.1	+0.7	Australian National	Australian National
061, S. Georgia Isl.	...	...	54°16'39.5147"S	36°29'17.4690"W	4.180	...	Astro	International
063, Dakar	14°44'39.8986"N	17°28'57.5476"W	14°44'44.23"N	17°29'04.41"W	26.28	+20.7	Adindan	Clarke 1880
064, Ft. Lamy	12°07'51.7410"N	344°57'53.7659"W	12°07'53.939"N	344°57'51.044"W	295.41	+23.6	Adindan	Clarke 1880
065, Hohenpeissenberg	47°48'07.009"N	348°58'31.4263"W	47°48'09.54"N	348°58'29.47"W	943.50	-0.6	European	International
067, Natal	05°55'37.4136"S	35°09'53.8003"W	05°55'37.74"S	35°09'57.03"W	40.63	+26.14	South American 1969	South American
068, Johannesburg	25°52'56.98"S	332°17'34.83"W	25°52'50.06"S	332°17'28.82"W	1523.8	...	Buffelsfont	Clarke 1880
069, Tristan	...	...	37°03'26.2572"S	12°19'06.4452"W	24.83	...	Astro 1968	International
072, Chieng Mai	18°46'06.149"N	261°01'44.877"W	18°45'47.50"N	261°01'51.62"W	308.4	...	Indian	Everest
073, Diego Garcia	07°20'58.5270"S	287°31'27.8444"W	7°20'58.53"S	287°31'27.84"W	3.85	...	1969 Astro	International
075, Mahé	04°40'11.614"S	304°31'06.617"W	4°40'10.31"S	304°31'06.02"W	588.98	...	Mahé 1971	Clarke 1880
111, Wrightwood	34°22'54.5368"N	117°40'50.5161"W	34°23'00.80"N	117°40'35.38"W	2284.41	-23.0	North American 1927	Clarke 1866

TABLE 15. Components of Vertical Deflections

Station	$\Delta\phi$	$\Delta\lambda$	η^*	cos ϕ
001	6.81"	-48.34"	-11.28	0.2334
002	-1.60"	7.37"	5.72	0.7768
003	-3.41"	-0.63"	-0.43	0.6796
004	14.51"	18.87"	11.43	0.6058
006	-1.26"	19.51"	6.78	0.3475
007	7.20"	10.13"	7.90	0.7797
008	-4.48"	-1.90"	-1.89	0.0955
009	-1.36"	9.46"	9.46	1.0000
011	-5.06"	-1.33"	-1.24	0.9353
012	-3.90"	-14.31"	-13.51	0.9439
013	-4.08"	9.44"	8.06	0.8537
015	2.29"	16.88"	13.62	0.8066
016	0.20"	18.34"	14.56	0.7939
020	-2.79"	-5.26"	-4.68	0.8896
022	-13.87"	-0.86"	-0.83	0.9689
023	-3.78"	-4.66"	-4.58	0.9830
031	-2.94"	3.23"	2.23	0.6894
032	0.34"	-28.10"	-23.87	0.8496
038	-13.28"	-2.21"	-2.09	0.9470
039	-0.31"	-0.79"	-0.72	0.9058
040	-13.89"	-15.97"	-15.61	0.9774
042	-6.78"	5.00"	4.94	0.9883
043	1.85"	-7.30"	-4.42	0.6048
044	-2.96"	-7.80"	-4.70	0.6016
045	15.63"	-39.61"	-37.17	0.9383
047	-2.48"	-2.38"	-2.36	0.9927
050	-7.21"	-16.45"	-7.01	0.4260
051	1.72"	1.08"	0.41	0.3811
052	-0.14"	-2.84"	-1.14	0.4022
053	-1.66"	-16.88"	-3.55	0.2105
055	-2.86"	-4.78"	-4.73	0.9903
059	17.23"	5.67"	5.66	0.9994
060	-1.88"	-9.96"	-8.60	0.8633
061	21.62"	21.63"	12.63	0.5838
063	2.03"	-4.66"	-4.51	0.9670
064	-0.65"	1.91"	1.87	0.9777
065	5.54"	5.53"	3.71	0.6717
067	1.32"	-1.69"	-1.68	0.9946
068	9.11"	7.59"	6.83	0.8997
069	27.35"	-11.75"	-9.38	0.7981
072	-23.07"	5.44"	5.15	0.9468
073	8.10"	11.04"	10.95	0.9918
075	4.37"	5.85"	5.83	0.9967
111	6.37"	18.49"	15.26	0.8253

Δ equals astro minus geodetic.
*$\eta = \Delta\lambda \cos\phi$.

A comparison between the XYZ coordinates given in Table 9 and the corresponding information computed from the survey data (Table 14) results in the translations Δx, Δy, Δz. These translations transform station by station the survey data into a mass-centered system.

Table 17 shows these results, the stations being grouped in terms of specific datums. Large differences in these translations for stations within a specific datum suggest distortions in such a datum.

In the column labeled N of Table 17 the geoid height used for the computation of the station shift components is given. At stations where such information was not available from the collected survey data the corresponding geoid heights from the combined solution (Table 16) were used, these cases being indicated by an asterisk.

Furthermore, a set of station shift components was computed on the basis of astronomical positions of the BC-4 stations where no other survey data were available. Here the computations were again based on geoid heights obtained from the combined solution, and furthermore, an ellipsoid with $f = 1:298.25$ and an equatorial radius of 6,378,130 was used. The resulting Δx, Δy, and Δz of shifts express therefore only the plumb line deflections tabulated in Table 15.

For datums for which more than one station is available, datum shift parameters were computed, allowance being made for an additional scale factor and an additional rotation in longitude in addition to the conventional three translations. These results are shown in Table 18. The smaller the indicated coordinate differences after datum shift, the more closely the survey result resembles the relative geometry as determined by satellite triangulation.

Because of the small number of stations belonging to a specific datum, it is not possible to compute meaningful datum shifts allowing an adjustment in the spatial orientation of the rotation axis of the individual datum ellipsoids, as desirable as such a test would be from the theoretical standpoint. Such a complete set of datum shift parameters will be computed for the North American Datum when the results of the satellite densification program in the area of the North American continent are completed.

The BC-4 world net is the result of a strictly three-dimensional geometric triangulation, including a scale derived

TABLE 16. Height of Geoid Above Ellipsoid (N)

Station	N Combined Solution Based on 6378130, m	N Anderle Solution, m	ΔN, m
1	13.379	7.30	+6.08
2	-45.758	-43.7	-2.05
3	-32.671	-29.70	-2.97
4	2.985	-3.40	+6.38
6	27.357	24.16	+3.20
7	55.569	51.87	+3.70
8	-38.495	-34.25	-4.25
9	11.947	15.90	-3.95
11	26.386	15.81	+10.58
12	0.837	15.08	-14.24
13	17.516	27.80	-10.28
15	-27.614	-26.80	-0.81
16	36.972	36.42	0.55
19	19.419	26.44	-7.02
20	-11.045	-11.20	0.16
22	30.007	30.83	-0.82
23	59.659	67.88	-8.22
31	-0.957	0.95	-1.91
32	-34.627	-40.30	5.68
38	-37.901	-41.20	3.30
39	-22.170	...	...
40	-34.237	-39.40	5.16
42	-13.813	-18.90	5.09
43	14.554	-0.65	15.20
44	35.891	...	...
45	-0.386	-3.54	3.15
47	61.944	65.56	-3.62
50	9.588	7.84	1.75
51	28.813	...	...
52	-7.245	...	...
53	-60.185	-58.20	-1.98
55	12.999	13.72	-0.72
59	21.764	22.95	-1.19
60	23.988	21.37	2.62
61	15.023	...	...
63	29.098	28.75	0.35
64	11.356	7.35	4.01
65	34.452	34.06	0.39
67	-2.342	-6.09	3.75
68	13.085	17.70	-4.62
69	20.602	...	...
72	-48.820	-44.12	-4.70
73	-76.765	...	...
75	-43.598	-39.18	-4.42
111	-32.149	...	...

$N = h - H$, where h is ellipsoid height and H is mean sea level elevation.
Σ = +3.33, and rms = ±5.57 for ΔN.

TABLE 17. Station Shifts

Station	Datum	ΔX, m	ΔY, m	ΔZ, m	N, m	Ellipsoid
002	North American	-15.464	-175.238	+170.683	-0.4	Clarke 1866
003		-15.073	-168.389	+176.173	-16.0	
004		-14.839	-224.661	+125.460	-46.0	
111		-14.909	-156.030	+174.079	-23.0	
023	Australian	-124.696	+59.448	+145.870	-4.6	Australian National
032		-122.122	+61.380	+148.912	+15.4	
060		-120.584	+58.544	+140.350	+0.7	
006	European	-95.289	+87.386	-130.319	+12.6	International
015		-102.814	+116.573	-157.106	-38.0	
016		-94.780	+97.941	-128.373	-16.6	
065		-98.045	+94.773	-130.038	-0.6	
042	Adindan	-175.031	+22.702	+207.848	-8.0	Clarke 1880
063		-159.895	+18.666	+211.616	+20.7	
064		-162.790	+18.035	+201.089	+23.6	
009	South American 1969	-62.026	-30.896	-38.650	+24.6	South American
019		-84.870	-10.993	-28.779	+13.0	
067		-79.113	+2.203	-44.415	+26.14	
001	Qornoq	+193.755	-152.336	-179.116	+32.0	International
007	SW Base	-146.464	-189.307	-85.530	+55.569*	International
008	Provisional South American 1956	-285.742	-124.472	-364.343	+3.0	International
011	Old Hawaiian	+89.609	+272.174	-204.940	+26.28	Clarke 1866
012	Astro 1952	+297.342	+62.206	+118.723	+0.837*	International
013	Tokyo	-112.208	-476.369	+643.232	+27.0	Bessel
022	American Samoa 1962	-75.859	-125.169	+431.583	+22.0	Clarke 1866
031	Geodetic 1949	+86.529	+29.100	+204.364	-0.957*	International
043	Provisional South Chile 1963	+4.265	-209.046	+104.397	+14.554*	International
045	LePonce Astro 1880	-750.581	-159.580	-507.541	-0.386*	Clarke 1880
047	Luzon	-72.235	+115.447	-115.971	+61.944*	Clarke 1886
055	Ascension Isl. 1958	-231.471	-111.769	+48.248	+12.999*	International
068	Buffelsfontein	-153.391	+130.351	-283.829	+13.085*	Clarke 1880
072	Indian	+230.419	-827.968	+291.150	-48.820*	Everest
075	Mahé 1971	+60.571	+197.879	-140.513	-43.598*	Clarke 1880
007	Astro	+12.302	+280.978	-173.013	+55.569*	Combined solution
012	Astro 1952	-58.951	+415.588	+113.310	+0.837*	a = 6378130
020	Astro 1967	+123.534	+85.205	+76.460	-11.045*	f = 1:298.25
038	Astro Isla Socorro	+107.336	-99.244	+386.616	-37.901*	f = 1:298.25
039	Astro 1967	+14.216	+17.322	+8.608	-22.170*	f = 1:298.25
040	Astro Anna 1965	-490.078	-32.066	+417.173	-34.237*	f = 1:298.25
044	Astro 1969	-118.468	-111.631	+55.102	+35.891*	f = 1:298.25
045	Astro LePonce	-1058.365	-479.038	-451.105	-0.386*	f = 1:298.25
050	Astro 1969	+283.896	+86.525	+95.174	+9.588*	f = 1:298.25
051	Astro 1969	-11.130	+49.721	-20.296	+28.813*	f = 1:298.25
052	Astro 1969	-34.580	+8.773	+1.786	-7.245*	f = 1:298.25
053	Astro Camp Area 1961/1962	-74.517	+95.634	+10.908	-60.185*	f = 1:298.25
059	Astro Christmas Isl. 1967	-84.514	-154.619	-528.955	+21.764*	f = 1:298.25
061	Astro	-669.022	-8.101	-390.231	+15.023*	f = 1:298.25
069	Astro 1968	-434.607	-392.099	-672.974	+20.602*	f = 1:298.25
073	ISTS Astro 1969	+313.175	+132.303	-246.794	-76.765*	f = 1:298.25

Δ equals combined solution minus survey parameter.
*N was obtained from combined solution (Table 16, combined solution) because of lack of corresponding survey data.

from classic geodetic surface measurements executed between several pairs of world net stations. Because the method of geometric satellite triangulation is based on absolute directions as obtained by interpolating the satellite position into the background of the surrounding field of fixed stars, the triangulation results can at best be only as accurate as the astronomical system of right ascension-declination itself. This situation holds for both the relative accuracy of the reference stars and the absolute accuracy of the astronomical reference system in its entirety. The photogrammetri triangulation, as a result of the high redundancy of data, should provide a result valid to about 1 part in 2 million in terms of the average station-satellite distance, in other words, station positions with an accuracy of ± 3 to ± 4 m in all three coordinates. The statistical information obtained as a by-product of the various data reduction steps indicates that the accuracy of the final result does not entirely fulfill the theoretical accuracy expectations. The statistically proven instability of the BC-4 camera system must be considered as a possible source of a slight systematic error, which in the adjustment algorithm is unavoidably distributed in accordance with the minimum principle for residual errors. The good agreement of the photogrammetric triangulation result with the measured base lines around the world indicates however that the final result is essentially free of significant bias errors. A comparison between the result of the geometric triangulation and the corresponding result obtained by dynamic satellite geodesy from Doppler data, as computed by the DMA and the Navy, shows excellent agreement in an overall sense but significant discrepancies in a few places on the globe. A combination of both results that respects fully the covariance of the photogrammetrically derived directions becomes possible by assuming a weighting of the dynamically determined coordinates in accordance with a station position mean error of ± 3.5 m. The only significant difference between the Navy-8D dynamically determined result and the geometric triangulation is in terms of scale, the indication being that the dynamic solution is based on a scale larger by 2 parts in a million. The

TABLE 18. Datum Shifts

Datum	Stations	Residual Coordinate Differences After Datum Shift			Datum Shift Parameters				
						Δλ Rotation +λ East	Translations		
		Δφ, m	Δλ East, m	Δh, m	Scalar	X to Y	ΔX, m	ΔY, m	ΔZ, m
North American	002	-1.9	-1.9	-2.4	1.0000000656	-0.7680"	-31.6	+171.1	+173.4
	003	+6.1	-0.5	-2.2					
	111	-2.6	+2.1	+4.6					
Australian	023	+1.2	+1.4	+1.6	0.9999999399	+0.0730"	-124.1	-61.0	+144.9
	032	+2.8	+0.3	-2.8					
	060	-4.8	-1.9	+1.1					
European	006	-0.1	-0.3	+0.2	0.9999991720	+0.7563"	-96.4	-78.9	-125.6
	016	-0.2	-0.3	+0.9					
	065	+0.4	+0.4	-1.1					
South American 1969	009	+5.4	+10.4	-3.4	0.9999949067	+0.7101"	-43.5	-1.9	-44.1
	019	-2.3	-13.5	-0.4					
	067	-3.3	+1.1	+3.7					
Adindan	042	+1.3	+0.6	-2.2	0.9999999794	-0.5231"	-162.6	-34.0	+206.9
	063	+5.1	-0.2	-0.6					
	064	-6.5	-0.4	+2.8					

geometric solution suggests a value of 6,378,130 m for the equatorial radius a of a best-fitting ellipsoid.

Acknowledgments. The worldwide geometric satellite triangulation program conducted from mid-1966 to the latter part of 1973 was a cooperative undertaking between the National Aeronautics and Space Administration, which designed and launched the target balloon, and the Defense Department, specifically the DMA, which contributed the major part in the funding for the observation and data reduction effort and assisted significantly in the field observation phase. The technical supervision of the program was with the National Geodetic Survey (NGS), a part of the National Ocean Survey, NOAA. NGS provided the major contribution in the data acquisition and was solely responsible for the data reduction and analysis. Specifically, the Geodetic Research and Development Laboratory (GRDL) of NGS was responsible for the technical and scientific aspects of the program. The management of the program was in the hands of L. W. Swanson of NGS. His outstanding and unwavering support during the solution of an endless number of practical problems in conducting this worldwide precision measuring program is thankfully acknowledged. Without the splendid cooperation of the international community this program could not have been conducted successfully. The cooperation of the nations that were asked for and provided station sites is hereby acknowledged. The participation in the actual field observation program by teams of the United Kingdom and the German Federal Republic contributed decisively to the required data bank. The measuring of the necessary scale lines by the geodetic agencies of Australia, Norway, Sweden, Denmark, German Federal Republic, Austria, and Italy and the contribution by France to the African scalar are thankfully mentioned in recognition of the fact that these results are essential for scaling the worldwide geometric triangulation. Last, but certainly not least, the dedication and contributions of the members of GRDL are mentioned; for a decade they have made their outstanding capabilities available for the solution of many theoretical and computer-oriented problems. Altogether, close to 200 employees of the aforementioned U.S. agencies have made their contribution to the program. All of them deserve thanks and recognition for their contributions.

REFERENCES

Altman, J. H., and R. C. Ball, On the spatial stability of photographic plates, *Photogr. Sci. Eng., 5,* 278–282, 1961.

Anderle, R. J., Transformation of terrestrial survey data to Doppler satellite datum, *J. Geophys. Res., 79,* this issue, 1973.

Bossler, J. D., *The SAO Star Catalog, Its Qualitative and Quantitative Value to the U.S.C.G.S Satellite Triangulation Program,* Environmental Science Services Administration, Institute for Earth Sciences, Geodetic Research Laboratory, Washington, D. C., 1966.

Hynek, J. A., On the effects of image motion on the accuracy of measurement of a flashing satellite, Research in Space Science, *Spec. Rep. 33,* 3 pp., Smithson. Inst. Astrophys. Observ , Cambridge, Mass., 1960.

Lundquist, C. A., and G. Veis (Eds.), *Geodetic Parameters for a 1966 Smithsonian Institution Standard Earth, Spec. Rep.* 200, vol. 3, p. 70, Smithsonian Astrophysical Observatory, Cambridge, Mass., 1966.

Nettelblad, F., *Studies of Astronomical Scintillation, Lund Observ. Publ. Ser. 2,* no. 130, Lund Observatory, Lund, Sweden, 1953.

Rinner, K., Systematic investigations of geodetic networks in space, *Annu. Tech. Rep. 91-591-EUC 3584,* Eur. Res. Office, Univ. of Graz, Graz, Austria, 1966.

Schmid, H., Satellite triangulation, in *The Proceedings of the Second International Symposium on the Use of Artificial Satellites for Geodesy,* edited by G. Veis, pp. 245–276, National Technical University, Athens, Greece, 1967.

Schmid, H., Triangulation mit Satelliten, in *Jordan-Eggert-Kneissl Handbuch der Vermessungskunde,* 10th ed., vol. 3a/3, *Photogrammetrie,* chap. 3, pp. 2081–2233, Metzler, Stuttgart, Germany, 1972.

Schmid, H., Three-dimensional triangulation with satellites, *Prof. Pap. 7,* Nat. Oceanic and Atmos. Admin., Rockville, Md., 1974.

Schmid, H., and E. Schmid, A generalized least squares solution for hybrid measuring systems, *Can. Surv., 9,* 27–41, 1965.

Wolf, H., *Computation of Satellite Triangulation by Spatial Fitting of the Orbit, German Geod. Comm. Ser. B,* no. 153, pp. 75–92, C. H. Beck, Munich, Germany, 1967.

(Received November 14, 1973,
revised July 22, 1974;
accepted July 22, 1974.)